220
Copy
RM L56H29

HADC
TECHNICAL LIBRARY
AFL 2811
Reg # 706
DEC 5 1956

TECH LIBRARY KAFB, NM
0144241

NACA RM L56H29

7716

RESEARCH MEMORANDUM

FREE-FLIGHT INVESTIGATION AT MACH NUMBERS BETWEEN 0.5 AND 1.7 OF THE ZERO-LIFT ROLLING EFFECTIVENESS AND DRAG OF VARIOUS SURFACE, SPOILER, AND JET CONTROLS ON AN 80° DELTA-WING MISSILE

By Eugene D. Schult

Langley Aeronautical Laboratory
Langley Field, Va.

CLASSIFIED DOCUMENT

This material contains information affecting the National Defense of the United States within the meaning of the espionage laws, Title 18, U.S.C., Secs. 793 and 794, the transmission or revelation of which in any manner to an unauthorized person is prohibited by law.

NATIONAL ADVISORY COMMITTEE FOR AERONAUTICS

WASHINGTON

November 29, 1956

TECH LIBRARY KAFB, NM

0144241

[redacted]

NATIONAL ADVISORY COMMITTEE FOR AERONAUTICS

RESEARCH MEMORANDUM

FREE-FLIGHT INVESTIGATION AT MACH NUMBERS BETWEEN 0.5 AND 1.7 OF THE ZERO-LIFT ROLLING EFFECTIVENESS AND DRAG OF VARIOUS SURFACE, SPOILER, AND JET CONTROLS ON AN 80° DELTA-WING MISSILE

By Eugene D. Schult

SUMMARY

A free-flight investigation of the zero-lift rolling effectiveness and drag of 18 roll-control arrangements on a cruciform 80° delta-wing missile-like configuration was conducted over the Mach number range between 0.5 and 1.7. Tests were made of deflected surfaces, spoilers, and inlet-air-jet devices in order to give evidence to simple theory for deflected surfaces and to determine some effects of chordwise location for spoilers and blowing direction and spanwise location for jets near the wing trailing edge.

The results demonstrated that all controls were satisfactory roll-producing devices except the canards located immediately forward of the main wings and spoilers at other than trailing-edge locations. A fuselage modification embodying the area-rule concept reduced the drag significantly and caused little change in the rolling effectiveness of a flap extending into the body indentation. For the jet controls, a comparison was made between the control forces generated by the various wing-jet combinations and the purely reactive thrust of the isolated jet blowing normal to the wing chord plane. The results indicate force magnifications of the order of 10 at subsonic speeds and 3 at supersonic speeds for jets blowing approximately normal to the wing surface from a line of orifices along the trailing edge. Spanwise-blowing jets directing air parallel to the wing surface and normal to the flight direction were not so efficient but were still more effective than a pure jet-reaction-type control. The rolling-effectiveness results are compared with simple theories which neglect all interference effects.

[redacted]

[redacted]

INTRODUCTION

Slender configurations employing highly swept, low-aspect-ratio wings have been of current interest in the missile design field for a number of reasons which involve reduced drag, the wing thermal-structural problem at high speeds, and missile portability aboard aircraft. At the present time, there is a general need for additional control information on such slender configurations. This need is due partly to the nature of the wing-body interference and its influence on simple methods for predicting effectiveness, and partly to the lack of data on controls for which little theory exists - notably spoilers and air-jet devices.

Some indication of the limit of present simplified methods for estimating the rolling effectiveness of deflected surfaces is provided by slender-configuration theory applied to all-movable-wing controls (ref. 1). Under the assumption that the flow remains attached, this theory demonstrates that the interference effects contributed by the body and vertical wings are small for body diameters less than 30 percent of the span. For this range of body diameters, therefore, it is conceivable that simple theories which neglect interference may be adequate insofar as the prediction of rolling effectiveness is concerned. It is of interest to confirm this experimentally for the deflected wings described previously and also for other low-span deflected surfaces which may be affected by interference or local flow separation.

Spoilers and air-jet controls hold promise from the low-actuating-force standpoint. Previous experiments with plain spoilers have shown the trailing-edge location to be most effective (ref. 2); however, in order to alleviate the high drag penalty, it has been suggested that ramp-type spoilers or plain spoilers located slightly behind the trailing edge be tested. Also of concern is the possibility of wing flutter induced by the spoiler at high speeds.

Recent investigations of air-jet controls consisting of a line of orifices in the wing surface have demonstrated that the jet effectiveness varies almost linearly with the jet mass-flow rate or flow momentum (refs. 3 to 5). These data also show that smaller orifices are generally the more effective for a given flow rate (possibly because of the greater stream penetration achieved). It is of interest to determine the effects, if any, of jet spanwise location and to evaluate the efficiency of spanwise-blowing arrangements wherein the jet is directed parallel to the wing surface normal to the flight direction. This installation eliminates the need for wing ducts and permits the use of extremely thin wings for reduced drag at high speeds.

The application of the area-rule concept to missiles has been considered not only as a means for reducing drag but also to obtain a better

distribution of fuselage volume for the installation of seeker components. Controlwise, it is important to determine what influence this modification may have on the effectiveness of a control partially submerged within the body indentation and in a region of possible flow separation.

In the present investigation, measurements were made between Mach numbers of 0.5 and 1.7 of the zero-lift rolling effectiveness and drag of a variety of controls on a slender, highly swept, missile-like configuration. The control problems enumerated above were investigated by means of the rocket-model technique. For comparative purposes, most of the controls had the same span. The deflected-surface results were compared with simple theory and plain trailing-edge spoiler data with two-dimensional estimates based on the wedge analogy of reference 6. The force data derived from the present and other tests of wing-jet controls were compared with the purely reactive thrust of the jet alone in an effort to correlate the available jet information and to evaluate the performance of the various wing-jet combinations.

SYMBOLS

A cross-sectional area, sq ft

b wing span, ft

c wing chord, ft

C_D total drag coefficient based on exposed wing area, $\frac{\text{Drag}}{qS_x}$

ΔC_D incremental drag coefficient attributed to controls

ΔC_L incremental lift coefficient due to control based on total planar wing area, $\frac{\text{Lift}}{qS}$

C_l rolling-moment coefficient based on total area of wings with controls attached, $\frac{\text{Rolling moment}}{qSb}$

C_{l_δ} rolling-moment coefficient per degree of surface deflection

C_{l_p} wing or configuration damping-in-roll coefficient based on total wing area, $\frac{\text{Damping moment}}{(pb/2V)qSb}$, per radian

C_μ jet-momentum coefficient based on total area of wings with controls attached, $\frac{m_j V_j}{qS}$

C_F jet-thrust force coefficient based on total jet-exit area, $\frac{\text{Thrust force}}{(P_t - P_a)A_j}$

d diameter, ft unless noted otherwise

F jet thrust force, lb

h vertical coordinate measured above wing surface normal to wing chord plane, ft unless noted otherwise

K_F total force magnification obtained with wing-jet combination expressed in terms of reactive thrust force of isolated jet directed normal to wing chord plane

l body length, ft

l_1, l_2 length and width, respectively, of slot, ft

Δl distance between orifices, ft

M Mach number, free stream unless noted otherwise

p model rolling velocity, radians/sec

pb/2V wing-tip helix angle, radians

P pressure, lb/sq ft

P_t stream stagnation pressure at inlet, lb/sq ft

q dynamic pressure, free-stream unless otherwise noted, $\frac{\gamma}{2}P_a M^2$ or $\frac{1}{2}\rho V^2$, lb/sq ft

r radial coordinate, dimensions as noted

S wing-plan-form area taken to model center line unless otherwise noted, sq ft

$(S_f/S)_x$ ratio of exposed control-surface area to exposed wing area

t	wing thickness, ft
V	velocity of model unless noted otherwise, ft/sec
w	jet mass-flow rate, total for wings with jets attached, slugs/sec
x	longitudinal coordinate, ft
y	spanwise coordinate measured from and normal to longitudinal axis, ft
$\beta = \sqrt{\lvert 1 - M^2 \rvert}$	
δ	control-surface deflection, average for all surfaces, per surface, deg
Δ	increment
ϕ	wing or flap section trailing-edge angle, positive for a sharp trailing edge, deg
γ	ratio of specific heats (C_p/C_v), 1.40 for air
ρ	stream density, slugs/cu ft
(AR)	aspect ratio
T.E.	trailing edge
C_1,C_2,C_3	constants

Subscripts:

a	ambient or static free-stream conditions
c	canard
f	flap or aileron
i	inlet plane or inboard extent of control
j	jet-exit plane (geometric characteristics of or stream conditions therein)
o	outboard extent of control

r wing root at fuselage juncture

s spoiler

DESCRIPTION OF MODELS

Nine of the 18 rocket-propelled test vehicles employed in this investigation are illustrated in the photographs of figure 1. Figure 2 presents the details of the basic test vehicle which was used in the majority of the tests. It consisted of 80° delta cruciform wings of aspect ratio 0.7 mounted on a pointed cylindrical fuselage. The basic wings had modified hexagonal sections approximately 2 percent thick at the wing-fuselage juncture and blunt trailing edges equal to one-half the maximum wing thickness. The basic wing was modified as shown so that three of the configurations employed thin-trailing-edge wings. The basic fuselage had an overall fineness ratio of 11, a nose fineness ratio of 3.5, and a diameter equal to 26 percent of the total wing span. One test was made of a modified fuselage shape which followed the area-rule concept for reduced drag and had, in addition, a better distribution of fuselage volume for installation of missile seeker components. Table I lists the body coordinates and figure 3 compares the cross-sectional area distributions for both the basic and modified fuselage configurations. In each case the wing sweep and exposed wing span were constants. Both models also had approximately the same maximum cross-sectional area and fuselage volume.

The roll controls comprised various arrangements of deflected surfaces, spoilers, and air jets (fig. 4). Most of these controls were of equal span and extended from the fuselage to the 75-percent station of the exposed wing semispan. Controls were located on all wings and were equally deflected to produce zero-lift roll.

The deflected-surface controls included inline canards, deflected main wings, plain flaps in conjunction with both fuselage shapes, split flaps, and detached surfaces located at two chordwise positions in the wing wake. The control of model 8 was arranged to simulate either a split flap, a spoiler ramp or, with minor corrections to the data to account for the slope of the trailing edge, a plain flap with extremely thick trailing edges.

The spoilers consisted of the ramp previously mentioned and three plain spoilers at chordwise locations forward of, at, and behind the wing trailing edge. The spoiler projections were equal and of the order of the local wing thickness. A small normal accelerometer (vibrometer) was embedded in one wing of the spoiler-mounted models to detect the presence of possible spoiler-induced flutter.

The air-jet controls consisted of simple inlet-jet arrangements using air obtained from the free stream. The air was directed either spanwise along or approximately normal to the wing surface near the trailing edge. Test variations were made in the spanwise placement and spanwise extent of the orifices and in the orifice area. The inlet frontal areas were equal for all configurations and occupied approximately 6 percent of the model frontal area.

FLIGHT-TESTING TECHNIQUE

The test measurements of zero-lift rolling effectiveness and drag were obtained by the rocket-model technique and covered the Mach number range between approximately 0.5 and 1.7. The flight tests were conducted at the Langley Pilotless Aircraft Research Station at Wallops Island, Va. A two-stage rocket propulsion system accelerated the model to the maximum test Mach number in approximately 3 seconds. During the 20-second time interval that followed, the model decelerated through the test Mach number range while measurements were made of the velocity with a CW Doppler velocimeter (radar) and of rolling velocity with spinsonde radio equipment. These data in conjunction with radiosonde information and space coordinates, obtained with a modified SCR-584 radar unit, permitted an evaluation of the Mach number M, the total drag coefficient C_D, and the wing-tip helix angle $pb/2V$ as functions of time. Also obtained during the flight tests of the spoiler-mounted models were time histories of the wing-bending acceleration in order to provide some indication of the possibility of spoiler-induced wing flutter.

The test Reynolds number varied with Mach number from approximately 2×10^6 to 1×10^7 per foot for all configurations (fig. 5).

ACCURACY AND CORRECTIONS

Calculations and flight-test experience indicate that the test results are accurate to within the following limits:

	Subsonic	Supersonic
M	±0.01	±0.01
$pb/2V$, radians	±0.003	±0.002
C_D	±0.003	±0.002

Slight corrections were made in the rolling-effectiveness data to account for small variations in wing incidence (from 0°) due to

construction tolerances. These variations in wing incidence were usually less than $\pm 0.03^{\circ}$. The corrections were applied by using the averaged measured wing incidence in conjunction with test data from model 2. In all cases these corrections were less than $\Delta pb/2V = \pm 0.001$ radian.

In order to compare the rolling effectiveness of the various deflected surfaces not tested at the same deflection, it was assumed that the effectiveness varied linearly with deflection. These data were therefore reduced to the form $\frac{pb/2V}{\delta}$, where δ is an average of the measured deflections of all four control surfaces. In this case the accuracy of measuring the angular deflection of the control surfaces is believed to be within $\pm 0.0083^{\circ}$ per foot of mean deflected-surface chord. The maximum deviation of measured flap deflection from the average for all four surfaces was usually less than $\pm 0.1^{\circ}$. The data were left in terms of the basic parameter $pb/2V$ for the spoiler controls which were tested at equal projection and for the air-jet controls tested in conjunction with equal inlet areas.

No corrections were made to account for the effects of model inertia about the roll axis on the measured rolling effectiveness when time variations in rolling velocity occurred. It was estimated that these variations from the steady-state roll condition were small and within the accuracy limits of the testing technique.

RESULTS AND DISCUSSION

The test results are presented as curves of the zero-lift rolling effectiveness plotted against Mach number in figures 6 to 13, jet-thrust coefficients and thrust-force magnifications against Mach number in figures 14 and 15, and drag coefficient against Mach number in figures 16 to 19. Discussed in order of their presentation are deflected surfaces, spoilers, and inlet-jet controls, all in connection with cruciform 80° delta-wing configurations. The tests were limited to a single deflection for each surface, to a constant projection for all spoilers, and to a constant inlet area for all jets. Estimates of the rolling effectiveness were based on the following equation for steady, single-degree-of-freedom roll:

$$\frac{pb}{2V} = \frac{C_l}{-C_{l_p}} = \frac{\left(C_{l_\delta}\right)\delta}{-C_{l_p}} \tag{1}$$

The rolling-moment coefficients, C_l and C_{l_p} were obtained from the various sources noted below. The effective control span used in estimating

C_l was exposed span, except for the deflected wings where total span was employed.

Rolling Effectiveness

Deflected-surface controls.- The data for all deflected surfaces are presented in figures 6 to 9.

Canards: Figure 6 shows that roll reversal was obtained by deflecting canards located immediately forward of and in line with the main wings. The measured data are presented in the basic form $pb/2V$ for $\delta_c = 6.06^\circ$. Results are compared with the calculated rolling effectiveness of the configuration assuming no interaction between canard and wing surfaces (ref. 1). From the increment between the curves, the estimated angle of effective downwash (or sidewash) from the canards was equivalent to a built-in negative wing incidence of approximately 0.8°. These results emphasize that canards followed by large wing areas are not satisfactory roll-producing devices in the usually accepted sense.

All-movable wings: In figure 7 the measured rolling effectiveness of differentially deflected wings, plain flaps, and detached surfaces are shown by the solid curves. Estimates based on available theory (refs. 1, 8, 9, 10, and 11) are noted by the broken curves. For the deflected wings, the results indicate that the effect of Mach number on rolling effectiveness is small; these results are in good agreement with the results of previous investigations on other wings (ref. 7). The experimental curve agreed well with the predictions of slender-wing theory for the planar wing alone (deflected to model center line). The predicted interference effects arising from the addition of the body and vertical wings are shown by theory to be small for this body diameter (0.26b). Simple strip theory overestimated the wing effectiveness by approximately 15 percent.

Plain flaps: The rolling effectiveness of the two flap-type ailerons of equal span but different chord are in good agreement at supersonic speeds with the level and trend predicted by linear theory applied to thin planar wings. (See fig. 7.) The measured results for both flaps are also compared with values based on zero-aspect-ratio theory for slender-wing control arrangements. The implication of this theory that control effectiveness is independent of flap chord near zero values of the reduced aspect ratio parameter $\beta(AR)$ appears to hold reasonably well near the limiting case ($M = 1.0$) for the larger-chord aileron. The lower effectiveness of the narrow-chord, thin-trailing-edge aileron at this Mach number may be caused by viscous effects not accounted for by the theory.

Detached surfaces: A comparison of the rolling power of plain flap-type ailerons with endplated detached surfaces of the same plan form

located in the wing wake shows the plain flap to be more effective at zero lift throughout the test Mach number range. (See fig. 7.) No significant improvement in the effectiveness of the detached surfaces was obtained by doubling the gap from one to two aileron chord widths. At subsonic speeds, the level for the detached surfaces was approximately two-thirds the value calculated for a two-dimensional isolated surface assuming a theoretical lift-curve slope of 2π for the surface and the theoretical damping-in-roll moment coefficient $(\pi(AR)/32)$ for the planar wing alone (ref. 10). At supersonic speeds, similar two-dimensional estimates of the effectiveness of an isolated surface were made by using linear theory; these values agreed so closely with the predicted curve for the plain flap (model 5) that for the sake of clarity they were omitted.

Split flaps and flap-section modification: Figure 8 compares the rolling power of plain and split flaps based on the flap deflections appropriate for each type of control. The results show that the split flaps were approximately half as effective as the plain flaps over the test Mach number range. Again results compared favorably with zero-aspect-ratio theory (ref. 10) at subsonic and transonic speeds and with linear theory (refs. 9 and 11) at supersonic speeds. The theoretical curves for the split flaps were derived on the basis of the local wing-flap mean-line deflection and presented in terms of upper-surface profile deflection.

The effect of modifying the section of the plain flap by increasing the trailing-edge thickness is shown in figure 9. The curve for the thick trailing-edge control was derived from the data of model 8 after applying a minor correction for base pressure acting on the inclined base. The base-pressure data were obtained from reference 12. The influence of the gap along the outer edge of the flap (model 3) was neglected in accordance with data published in reference 13. Results show that increasing the trailing-edge thickness beyond the hinge-line thickness generally improved the flap effectiveness. An estimate of this improvement at supersonic speeds is obtained by correcting linear theory (ref. 9) or data for the other flap section for the two-dimensional effects of flap trailing-edge angle (ref. 14) using Busemann's third-order approximation of two-dimensional flow. This correction factor, derived in reference 14 and applied herein to C_{l_δ}, is as follows:

$$\frac{\left(C_{l_\delta}\right)_\phi}{\left(C_{l_\delta}\right)_{\phi=0}} = \left[1 - \left(\frac{C_2}{C_1}\right)\phi + \frac{3}{4}\left(\frac{C_3}{C_1}\right)\phi^2\right]$$

The trailing-edge angle ϕ is expressed in radians and the constants C_1, C_2, and C_3, which depend primarily on Mach number, may be obtained from

the calculations of reference 14. The estimates are shown to be in good agreement with experimental results.

Plain flap with fuselage modification: Figure 10 illustrates the effect of a change in fuselage shape on plain-flap rolling effectiveness. Flap plan form and the fraction of exposed span occupied by the flap were identical in both cases. It is noteworthy that extending the flap into the body indentation and into a region of possible flow separation had little influence on the rolling effectiveness. This implies, however, that, if flow separation had occurred, the reduction in flap effectiveness was proportional to a reduction in the damping in roll of the configuration due to the fuselage modification. (See eq. 1.) In the present case, approximately a third of the flap span was screened by the maximum diameter station of the modified fuselage.

Spoiler controls.- Figure 11 presents some effects of spoiler shape and chordwise location. Span and projected height remained constant. The ramp (model 8) is seen to be about half as effective at subsonic speeds and almost equally effective at supersonic speeds as the plain spoiler (model 9). The most satisfactory chordwise location for the plain spoiler was at the trailing edge which agrees with other spoiler data on wings of lesser sweep (ref. 2). A more forward chordwise location (model 11) caused roll reversal, probably because of the mechanics of the flow reattachment to the wing behind the spoiler; similarly, the rear open-gap position (model 10), suggested as a means for reducing drag, was relatively ineffective at supersonic speeds.

A subsonic estimate of the ramp effectiveness, based on the same theory employed in connection with the split flap (fig. 8) is repeated in figure 11. At supersonic speeds the symbols show corresponding two-dimensional estimates for the plain and ramp spoilers based on control loadings from plane-shock relations and free-stream flow conditions. For the plain spoiler, the wedge analogy of reference 6 was employed to determine the extent of the control pressure field acting on the wing forward of the spoiler. This method presumes the presence of a wedge, similar to the ramp on model 8, which occupies the region forward of the spoiler. The "wedge" apex angle and chord are adjusted according to local flow conditions so that the pressure rise produced by the wedge matches the critical rise necessary for boundary-layer separation forward of a step surface discontinuity. In the present case, the experimental pressure coefficients necessary to separate a turbulent boundary layer were obtained from reference 15 and substituted into plane-shock relations (ref. 16) to determine the wedge angles and corresponding control "surface" areas. The loadings were then expressed in terms of rolling effectiveness by means of equation (1) by using theoretical values of C_{l_p} for the cruciform configuration (ref. 1). The resulting semiempirical estimates are shown to agree well with test data. As a matter of interest, the wedge angles were of the order of 9°, 11°, and 13° at $M = 1.5$, 1.7, and 2.0, respectively.

The results of the vibrometer tests to obtain indications of spoiler-induced flutter were negative. No oscillations were apparent in the variation of wing bending acceleration against time.

Air-jet controls.- The rolling effectiveness of the various inlet-jet devices are presented in figures 12 and 13. Air was supplied to the jets from simple inlets of equal intake area in all cases.

Jets blowing normal to wing: Figure 12 shows the variations with Mach number of the rolling effectiveness of air jets blowing approximately normal to the wing surface. In addition to present data, some curves for a full-span jet configuration of similar orifice pattern (ref. 3) and for a configuration with jets forward of the trailing edge (ref. 4) are presented. The latter model was originally part of the present investigation but, because of structural failure during test, no free-flight data were obtained. Results show that the effectiveness of inboard jets increases almost linearly with increasing span at supersonic speeds (models 14 and 12 and ref. 3). In the same speed range, the higher effectiveness of the outboard jet location over its corresponding inboard location can be accounted for by considering the difference in moment arms (models 13 and 14). Superposition of the effectiveness of adjacent spanwise elements to obtain the effectiveness of a larger span is not practical for this configuration (models 12, 13, and 14); this is probably due to the reduction in unit-jet flow rate resulting from the increase in manifold flow loss with increased exit-to-inlet area ratio. Jets forward of the trailing edge were ineffective, as were plain spoilers at the same position (fig. 11).

Jets blowing spanwise along wing: The arrangements of jets blowing spanwise along the wing were considered an end point for jet devices which affect the flow over the wing. Although the reactive thrust component of the jet available for control purposes is small, it was believed that this disadvantage might be offset by the simplification achieved through elimination of wing ducts. Two methods for obtaining proportional control were tested in connection with the outboard jet configuration: (1) a constant-flow system (A_j/A_i = Constant) where air was ejected at differential rates to both upper and lower surfaces (models 15 and 17), and (2) a variable-flow system ($A_j/A_i \neq$ Constant) where the flow rate to one surface was controlled by adjusting the exit port area (models 15 and 16). Results shown in figure 13 indicate that the second method results in a more linear increase in rolling effectiveness with increased net exit area over the entire speed range of the test. A comparison of the relative effectiveness of the jets blowing normal to the wing and jets blowing spanwise and parallel to the wing can be gained from the curves of reference 3 (fig. 12) and model 15 (fig. 13). It will be seen that this comparison, based on approximately equal jet exit areas, shows both types are nearly equally effective at supersonic speeds. The inboard spanwise blowing configuration, consisting simply of a pair of turning vanes (model 18) was about two-thirds as effective as the outboard arrangement (model 15).

Jet thrust-force magnification: A determination was made of the force magnifications produced by the various wing-jet combinations in order to correlate the present results with other jet-control information and to provide a realistic basis for comparing the performance of normal- and spanwise-blowing arrangements. The force magnification K_F is defined as the ratio of the incremental normal force generated by the wing-jet combination to the normal force possible from the purely reactive thrust of the isolated jet blowing normal to the wing chord plane. It seems reasonable to assume that these magnifications are applicable over a fairly wide range of jet flow conditions since both the jet effectiveness and thrust vary almost linearly with the jet momentum. The present correlation, which covered a wide range of jet-flow conditions, tends to substantiate this assumption.

In the calculations described in the appendix, the values of K_F were derived from incremental lift, rolling moment, and rolling effectiveness information and from thrust measurements of the manifold-orifice configuration. Differences in the spanwise location of the jet were taken into account. The jet thrust coefficients were determined from ground tests of the various duct systems and are presented in figure 14. A comparison of the actual and ideal thrust coefficients (fig. 14(b)) indicates considerable flow loss within the manifold, particularly for those manifolds having normally blowing jet arrangements. These losses increased with increased ratio of exit area to inlet area (fig. 14(c)), which might be expected because of the increased flow velocity inside the manifold.

The thrust coefficients were applied to actual flight conditions experienced by the model by employing theoretical free-stream stagnation pressures at the inlet and ambient free-stream conditions at the jet exit. It should be recognized that the thrust of the isolated jet as determined by these calculations and used in K_F to correlate the data represents an idealized case and is not necessarily the actual thrust of the jet in combination with the wing. This difference in thrust arises from the difference between the assumed ambient pressure at the jet exit and the actual local wing back pressure which, because of jet effects, exists as part of the wing pressure field to produce force magnification. If actual wing back pressures were substituted into the calculations, the estimated thrust would probably be somewhat lower and the estimated force magnification somewhat higher than reported herein. It is believed, however, that the present usage of the isolated normal jet thrust in determining the force magnification gives a more realistic expression of the performance of the wing-jet combination.

Derived values of K_F against Mach number are presented in figure 15. All free-flight effectiveness data on jets blowing approximately normal to the wing surface correlate fairly well at supersonic speeds on the basis of differences in jet thrust and control moment arm (fig. 15(a)). At high

subsonic speeds, however, considerable scatter is evident due largely to the changes in orifice pattern; the smaller orifices or ratios of orifice diameter to spacing were apparently more effective aerodynamically. The average thrust magnification is of the order of 10 at subsonic speeds and decreases to 3 at supersonic speeds. Jets blowing spanwise and parallel to the wing surface are less efficient for a given flow rate than the normally blowing type although still more effective than a pure jet-reaction control ($K_F = 1$). It will be recalled that comparing jet types on a nearly equal exit-area basis (figs. 12 and 13) revealed only small differences in jet effectiveness; this is attributed to the higher flow rates resulting from the lower manifold losses for the spanwise-blowing arrangement (fig. 14(b)).

In figure 15(b) the free-flight results are seen to agree generally with values of K_F determined from referenced lift and rolling-moment data. For referenced configurations having inlets, the calculations were based on the thrust information presented in figure 14(c). When external air was employed for the jets, K_F was estimated from the slopes of the curves of the lift or rolling-moment data against jet momentum, taken near zero momentum coefficient. Figure 15(c) compares free-flight results for 80° delta wings with magnifications obtained on other plan forms (refs. 5, 17, and 18). The higher values in each case symbolize the data for the smaller orifices or data obtained at slight angles of attack. The results are in good agreement at transonic speeds.

It appears from the results of figure 15(a) that spanwise-blowing jets may have promise in reducing the landing speed or attitude of existing airplanes having low-aspect-ratio wings. For a configuration employing tip-mounted, forward, underslung engines equipped with jet-exhaust deflectors, it seems possible that considerable lifting force in excess of that obtained from jet reaction alone could be made available by directing all or part of the engine exhaust horizontally inboard under the wing. This lift increment might be further increased by shaping the fuselage sides to redirect the jet downward. While not so effective as downward-directed jets along the trailing edge, it would appear that this type of circulation control would offer a simpler installation, since no wing ducts are required, and may, in addition, provide some degree of lateral control by differential throttle manipulation. Further tests will be required, however, to evaluate fully the operational as well as the stability and control aspects of this arrangement in connection with an airplane-type configuration.

Drag

General.- Figure 16 presents the measured total drag coefficients, based on exposed wing area, of the test configurations with deflection-type controls. Also presented is the drag contribution of the body alone

from reference 19 based on the same characteristic area. No corrections have been made in the data to account for the induced-drag increment due to roll inasmuch as theoretical estimates for model 2 show that this increment is less than 0.001 (ref. 10). Results demonstrate that the thick trailing edges nearly doubled the incremental drag of the wing (models 3 and 5). Increasing the aileron trailing-edge thickness significantly increased the drag of the plain aileron relative to the clean wing (models 2, 3, and 8).

Figure 17 shows the drag reduction obtained by modifying the fuselage via the area-rule concept. In each case the drag coefficients are based on the exposed wing area of the basic configuration (model 3). The maximum cross-sectional area and fuselage volume remained essentially constant for both models (fig. 3).

Figure 18 presents the drag coefficients for the spoiler controls relative to the drag of the so-called clean configuration (model 2) and the body alone. It can be seen that projecting the plain spoiler almost doubled the total drag of the wing-body configuration at all test Mach numbers. For the same projected height, the incremental drag of the ramp was less than half that of the plain spoiler. Drag curves for the air-jet configurations are shown in figure 19 relative to the drag of the clean configuration and the body alone. It can be seen that the incremental drag of the inlet-jet control was not affected to a large extent by variations in the jet span or flow rate; this is in agreement with other data (refs. 3 to 5).

Drag comparison of controls.- A review of the preceding data demonstrates that the higher levels of rolling effectiveness obtained with certain controls were frequently accompanied by large drag penalties. It may be of interest, for high-speed missiles, to show the drag penalty of each control type at a given level of effectiveness, even though, for short-range applications, drag is usually of secondary importance compared with other control characteristics.

Figure 20 presents plots at three test Mach numbers of the rolling-effectiveness parameter against the incremental drag coefficient ΔC_D for the various controls. The incremental drag in each case was obtained by subtracting from the total drag the drag of the clean configuration (model 2). In interpreting the results for ailerons and spoilers it is assumed for purposes of comparison that both rolling effectiveness and drag are linear functions of control deflection so that a straight line between the origin and each test point defines the curve of increasing control deflection for that control. For jets, on the other hand, the jet inlet constitutes an essentially fixed drag penalty so that a straight line between the origin and the test point describes the effect of an increasing inlet frontal area for a given ratio of inlet area to jet-exit area; in this case, it is assumed that the incremental drag of the inlet, the inlet flow rate, and the jet effectiveness are all proportional to the intake area.

The results for this wing section substantiate the concept that the most effective controls judged on a drag basis are movable wings and plain flaps, followed in order by split flaps or ramp spoilers, plain spoilers, and finally inlet-air-jet devices. At transonic speeds, the air jets were equally effective as split flaps. Obviously, the use of other wing sections tailored to the control would alter this picture, particularly for spanwise-blowing jets adaptable to thin wing sections, or for jets energized by a source other than inlets.

CONCLUSIONS

A free-flight investigation of the zero-lift rolling effectiveness and drag of deflected surfaces, spoilers, and two types of inlet-air-jet arrangements on a cruciform 80° delta-wing missile-like configuration was conducted by means of the rocket-model technique for Mach numbers between 0.5 and 1.7. The following conclusions were obtained:

1. The results demonstrated that all controls tested were suitable roll-producing devices except the canards immediately forward of the main wings and spoilers away from the trailing edge. Detached surfaces in the wing wake were about half as effective at zero lift as plain flaps of the same plan form.

2. A fuselage modification embodying the area-rule concept reduced the drag significantly and caused little change in the rolling effectiveness of a flap extending into the body indentation.

3. Experimental results substantiated the predictions of slender-wing theory for the control effectiveness of all-movable wings throughout the test speed range. When interference effects were neglected, good estimates of the flap effectiveness were obtained at supersonic speeds with linear theory and for the larger-chord flap at sonic speeds with zero aspect-ratio theory.

4. Spoiler effectiveness at supersonic speeds compared favorably with two-dimensional and semiempirical estimates. There was no indication of spoiler-induced flutter.

5. A correlation of the jet-effectiveness data with the thrust force alone of the isolated jet turned normal to the wing chord plane revealed force magnifications of the order of 10 at subsonic and 3 at supersonic speeds for jets blowing approximately normal to the surface from orifices along the trailing edge. Spanwise blowing was not as effective, the magnifications being of the order of 3.0 and 1.5, respectively. Aside from basic moment arm considerations, there was no effect of spanwise placement of jets blowing normal to the surface.

6. A comparison of control types on a drag basis substantiates that all-movable wings and flaps were most effective for a given drag penalty.

Langley Aeronautical Laboratory,
National Advisory Committee for Aeronautics,
Langley Field, Va., August 13, 1956.

APPENDIX

WING-JET THRUST-MAGNIFICATION RATIO

The factor K_F is herein defined simply as the ratio of the incremental normal force produced by any wing-jet combination to the normal force available from thrust alone of the isolated jet blowing normal to the wing chord plane. It was determined as a function of Mach number from the experimental data of present and other tests in an effort to correlate the data and to provide the designer with a practical means for estimating or evaluating the performance of jet-control-wing combinations.

In the correlation the values of K_F were determined near zero angle of attack from referenced incremental-lift and rolling-moment data and from free-flight rolling-effectiveness (pb/2V) data by means of the following relations:

$$K_F = \frac{\Delta C_L qS}{F} \tag{A1}$$

$$K_F = \frac{C_l qSb}{Fy} \tag{A2}$$

and, for steady-state roll,

$$K_F = \frac{\left(-C_{l_p}\right)(pb/2V)qSb}{Fy} \tag{A3}$$

The characteristic thrust moment arm y is taken as the semispan ordinate from the roll axis to the midjet-span station for the jets blowing approximately normal to the wing and to the jet-exit plane for jets blowing spanwise and parallel to the wing. The damping-in-roll coefficient C_{l_p} for the 80° delta free-flight configurations were calculated from theory (ref. 1), these values being in good agreement with the experimental results of reference 4. The jet thrust force F was determined experimentally in most cases for the actual manifold in order to eliminate possible effects arising from differences in flow losses associated with differences in the manifold shape or the orifice size and arrangement.

For the inlet-jet devices the thrust coefficients were obtained as in reference 3. The manifold assembly with a small total-pressure tube

installed in the inlet plane was placed on a force balance and connected to a compressed-air supply by means of a straight flexible duct. Total normal-force measurements were obtained for a range of inlet stagnation-pressure ratios P_t/P_a between approximately 1.2 and 4 atmospheres and reduced to coefficients by the convenient relation

$$C_F = \frac{F}{(P_t - P_a)A_j} \tag{A4}$$

Figure 14 presents typical variations of the measured thrust coefficient against pressure ratio and ratio of exit area to inlet area for the present test and other jet arrangements. The results are compared with the ideal thrust coefficients for a convergent nozzle by considering the nozzle entrance plane to correspond to the manifold inlet. The curve defining the ideal thrust coefficient of a compressible gas emerging from the nozzle after expanding isentropically to the nozzle exit from stagnation conditions upstream was derived from the jet-thrust equation based on steady-flow impulse, momentum, and pressure relations:

$$F = m_j V_j + A_j(P_j - P_a) \tag{A5}$$

For subsonic jets, where the equality of P_j and P_a eliminates the pressure term, the ideal thrust coefficient becomes

$$C_{F_{ideal}} = \frac{m_j V_j}{(P_t - P_a)A_j} = \frac{\rho_j V_j^2}{(P_t - P_a)} = \frac{2q_j}{(P_t - P_a)} = \frac{\gamma M_j^2}{(P_t/P_a - 1)}$$

At subsonic speeds the ideal jet Mach number at the nozzle exit may be related to the upstream stagnation pressure by means of the following expression (from ref. 16):

$$P_t/P_a = \left[1 + \left(\frac{\gamma - 1}{2}\right)M_j^2\right]^{\frac{\gamma}{\gamma-1}}$$

Substituting this expression for M_j into the preceding equation for $C_{F_{ideal}}$ results in

$$C_{F_{ideal}} = 7\left[\frac{\left(P_t/P_a\right)^{0.286} - 1}{P_t/P_a - 1}\right] \quad . \; . \; . \; P_t/P_a \leqq 1.89 \qquad \text{(A6)}$$

when $\gamma = 1.4$. Near zero-flow conditions the value of this expression approaches the incompressible-flow value of 2.0 for a convergent nozzle obtained from Bernoulli's equation.

For choked nozzles $\left(P_t/P_a \geqq 1.89,\ M_j = 1.0, \text{ and } P_j = 0.528P_t\right)$ it can be shown that the ideal thrust coefficient for a convergent nozzle reduces to

$$C_{F_{ideal}} = \frac{2P_t\left(\frac{2}{\gamma + 1}\right)^{\frac{1}{\gamma-1}} - P_a}{\left(P_t - P_a\right)}$$

Dividing numerator and denominator by P_a and letting $\gamma = 1.4$ yields

$$C_{F_{ideal}} = \left[\frac{1.27P_t/P_a - 1}{P_t/P_a - 1}\right] \quad . \; . \; . \; P_t/P_a \geqq 1.89 \qquad \text{(A7)}$$

A comparison of actual and ideal coefficients in figure 14 indicates considerable friction loss within the manifold, particularly for the vertically blowing devices having large exit-to-inlet area ratios.

In order to relate the above coefficients to free-stream conditions at a given Mach number, the following identity was substituted into equation (A4):

$$\left(P_t - P_a\right) = 2q\left(\frac{P_t/P_a - 1}{\gamma M^2}\right)$$

Values of the free-stream stagnation pressure ratio P_t/P_a theoretically available at the inlet face were calculated from the conventional pitot equations (ref. 16) which, at supersonic speeds, assume the presence of a normal shock forward of the inlet.

Collecting terms by substituting the preceding relations for jet thrust into equations (A1), (A2), and (A3) and letting $y' = y/\frac{b}{2}$, yields

$$K_F = \left(\frac{\Delta C_L}{2C_F}\right)\left(\frac{S}{A_j}\right)\left(\frac{\gamma M^2}{P_t/P_a - 1}\right) \tag{A8}$$

$$K_F = \left(\frac{C_l}{y'C_F}\right)\left(\frac{S}{A_j}\right)\left(\frac{\gamma M^2}{P_t/P_a - 1}\right) \tag{A9}$$

$$K_F = \left(\frac{-C_{l_p}}{y'C_F}\right)\left(\frac{pb/2V}{A_j/S}\right)\left(\frac{\gamma M^2}{P_t/P_a - 1}\right) \tag{A10}$$

For referenced jet configurations tested with air from an external source, the value of K_F was obtained from the slopes of the data curves $\frac{\partial C_L}{\partial C_\mu}$, and $\frac{\partial C_l}{\partial C_\mu}$ multiplied by $\frac{2}{y'}$, taken near zero values of the momentum coefficient C_μ. This presumes that near zero momentum coefficient the jets are subsonic so that C_μ reflects the actual available jet thrust in combination with the wing in accordance with equation (A5). For completeness, it should be mentioned that the data coefficients and C_μ are necessarily based on the same referenced area.

REFERENCES

1. Adams, Gaynor J., and Dugan, Duane W.: Theoretical Damping in Roll and Rolling Moment Due to Differential Wing Incidence for Slender Cruciform Wings and Wing-Body Combinations. NACA Rep. 1088, 1952.

2. Wiley, Harleth G.: A Wind-Tunnel Investigation at High Subsonic Speeds of the Lateral Control Characteristics of Various Plain Spoiler Configurations on a 3-Percent-Thick 60° Delta Wing. NACA RM L54D01, 1954.

3. Schult, Eugene D.: A Free-Flight Investigation at High Subsonic and Low Supersonic Speeds of the Rolling Effectiveness and Drag of Three Spoiler Controls Having Potentially Low Actuating-Force Requirements. NACA RM L55G11a, 1955.

4. Turner, Thomas R., and Vogler, Raymond D.: Wind-Tunnel Investigation at Transonic Speeds of a Jet Control on an 80° Delta-Wing Missile. NACA RM L55H22, 1955.

5. Vogler, Raymond D., and Turner, Thomas R.: Wind-Tunnel Investigation at Transonic Speeds of a Jet Control on a 35° Swept Wing - Transonic-Bump Method. NACA RM L55K09, 1956.

6. Mueller, James N.: Investigation of Spoilers at a Mach Number of 1.93 To Determine the Effects of Height and Chordwise Location on the Section Aerodynamic Characteristics of a Two-Dimensional Wing. NACA RM L52L31, 1953.

7. Strass, H. Kurt, Stephens, Emily W., Fields, Edison M., and Schult, Eugene D.: Collection and Summary of Flap-Type-Aileron Rolling-Effectiveness Data at Zero Lift As Determined by Rocket-Powered Model Tests at Mach Numbers Between 0.6 and 1.6. NACA RM L55F14, 1955.

8. Strass, H. Kurt, and Marley, Edward T.: Rolling Effectiveness of All-Movable Wings at Small Angles of Incidence at Mach Numbers From 0.6 to 1.6. NACA RM L51H03, 1951.

9. Tucker, Warren A., and Nelson, Robert L.: Theoretical Characteristics in Supersonic Flow of Two Types of Control Surfaces on Triangular Wings. NACA Rep. 939, 1949. (Supersedes NACA TN's 1600 and 1601 by Tucker and TN 1660 by Tucker and Nelson.)

10. DeYoung, John: Spanwise Loading for Wings and Control Surfaces of Low Aspect Ratio. NACA TN 2011, 1950.

11. Piland, Robert O.: Summary of the Theoretical Lift, Damping-in-Roll, and Center-of-Pressure Characteristics of Various Wing Plan Forms at Supersonic Speeds. NACA TN 1977, 1949.

12. Morrow, John D., and Katz, Ellis R.: Flight Investigation at Mach Numbers From 0.6 to 1.7 To Determine Drag and Base Pressures on a Blunt Trailing-Edge Airfoil and Drag of Diamond and Circular-Arc Airfoils at Zero Lift. NACA TN 3548, 1955. (Supersedes NACA RM L50E19a.)

13. Sandahl, Carl A., and Strass, H. Kurt: Comparative Tests of the Rolling Effectiveness of Constant-Chord, Full-Delta, and Half-Delta Ailerons on Delta Wings at Transonic and Supersonic Speeds. NACA RM L9J26, 1949.

14. Tucker, Warren A., and Nelson, Robert L.: Theoretical Characteristics in Supersonic Flow of Constant-Chord Partial-Span Control Surfaces on Rectangular Wings Having Finite Thickness. NACA TN 1708, 1948.

15. Lange, Roy H.: Present Status of Information Relative to the Prediction of Shock-Induced Boundary-Layer Separation. NACA TN 3065, 1954.

16. Ames Research Staff: Equations, Tables, and Charts for Compressible Flow. NACA Rep. 1135, 1953. (Supersedes NACA TN 1428.)

17. Lowry, John G., and Turner, Thomas R.: Low-Speed Wind-Tunnel Investigation of a Jet Control on a 35° Swept Wing. NACA RM L53I09a, 1953.

18. Lowry, John G.: Recent Control Studies. NACA RM L55L22a, 1956.

19. Hart, Roger G.: Effects of Stabilizing Fins and a Rear-Support Sting on the Base Pressures of a Body of Revolution in Free Flight at Mach Numbers From 0.7 to 1.3. NACA RM L52E06, 1952.

TABLE I.- BODY COORDINATES

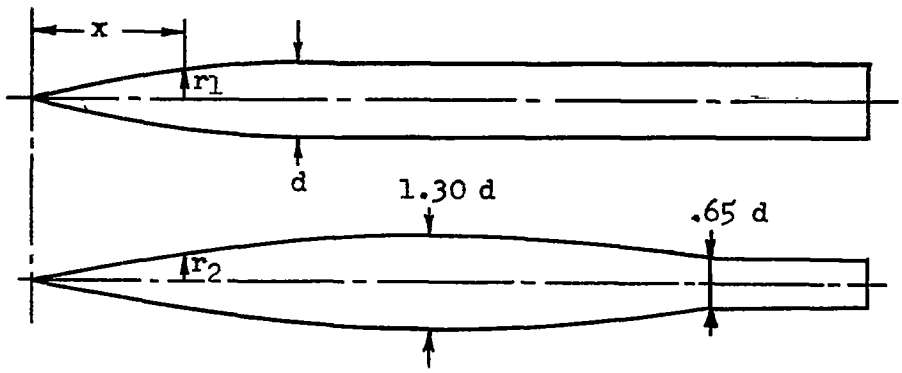

x, in.	r_1, in.	r_2, in.
0	0	0
2.50	0.61	0.61
5.00	1.15	1.15
7.50	1.58	1.58
10.00	1.96	1.96
12.50	2.26	2.32
15.00	2.44	2.62
17.50	2.50 (max.)	2.87
20.00	↓	3.05
23.00	↓	3.19
26.44	↓	3.25 (max.)
30.00	↓	3.19
35.00	↓	2.90
40.00	↓	2.16
44.83	↓	1.625
50.00	↓	↓
55.00	↓	↓

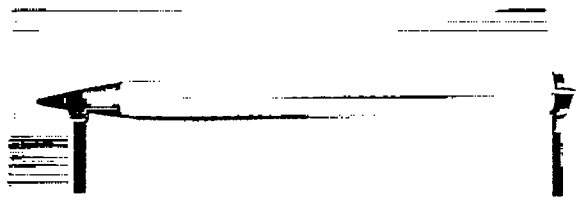

Model 1

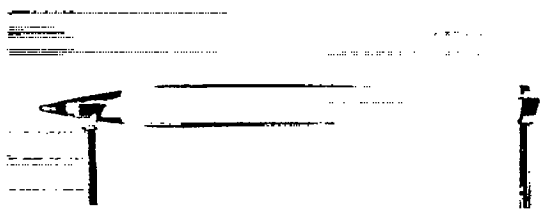

Model 2

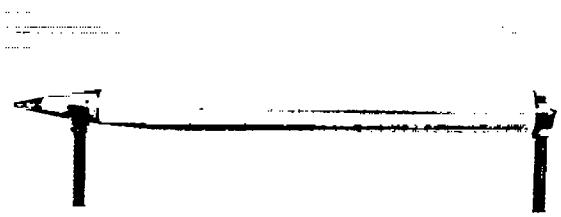

Model 3

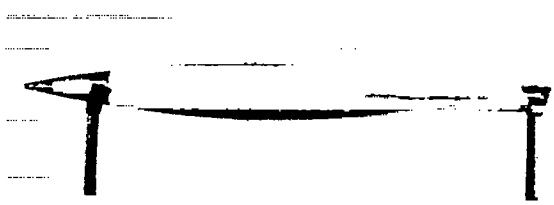

Model 4

(a) Closeup views of several models. L-95777

Figure 1.- Photographs of several of the test vehicles employed in the present investigation.

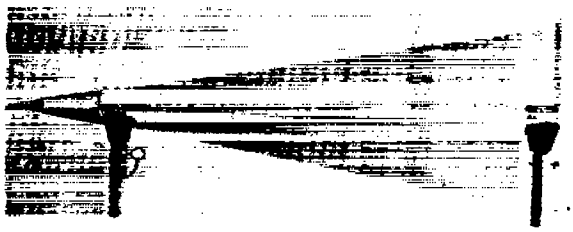

Model 5

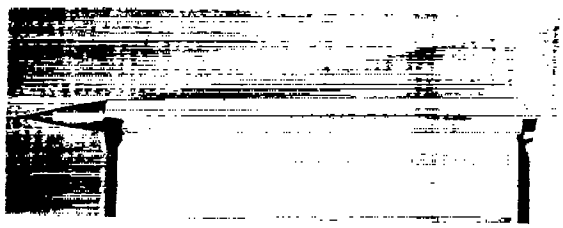

Model 6

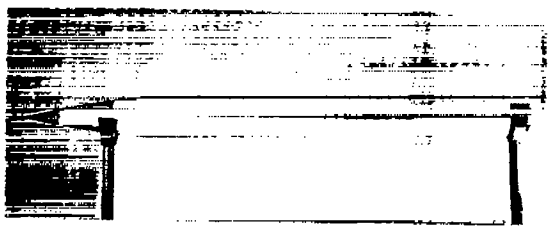

Model 9

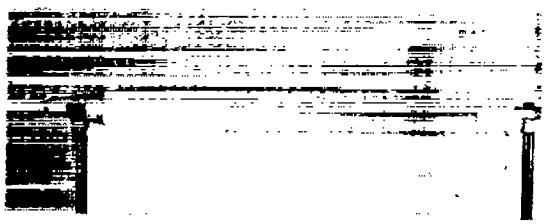

Model 12

(a) Concluded.

L-95778

Figure 1.- Continued.

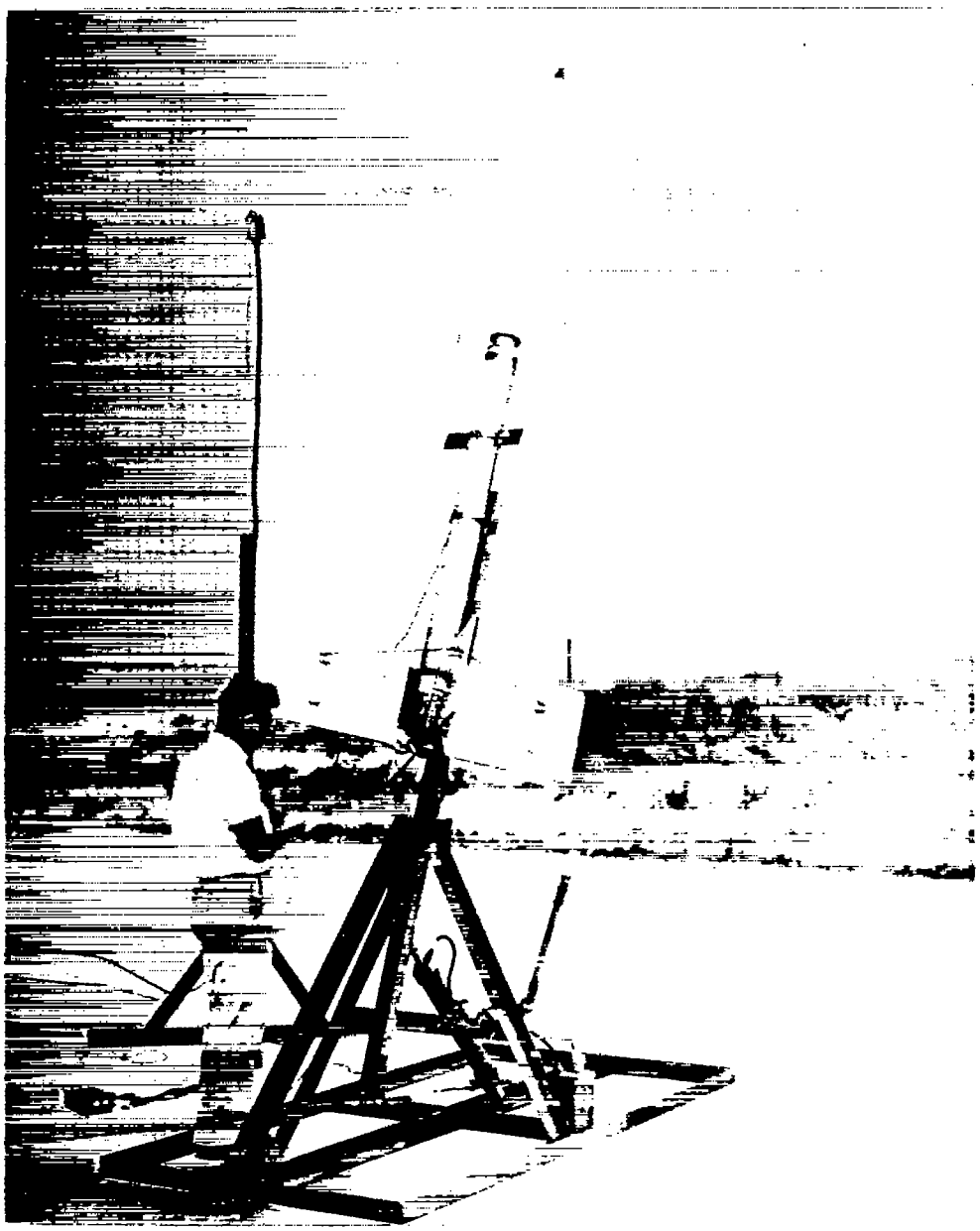

L-90168.1

(b) Model 15 mounted with booster on launching stand and being prepared for flight test.

Figure 1.- Concluded.

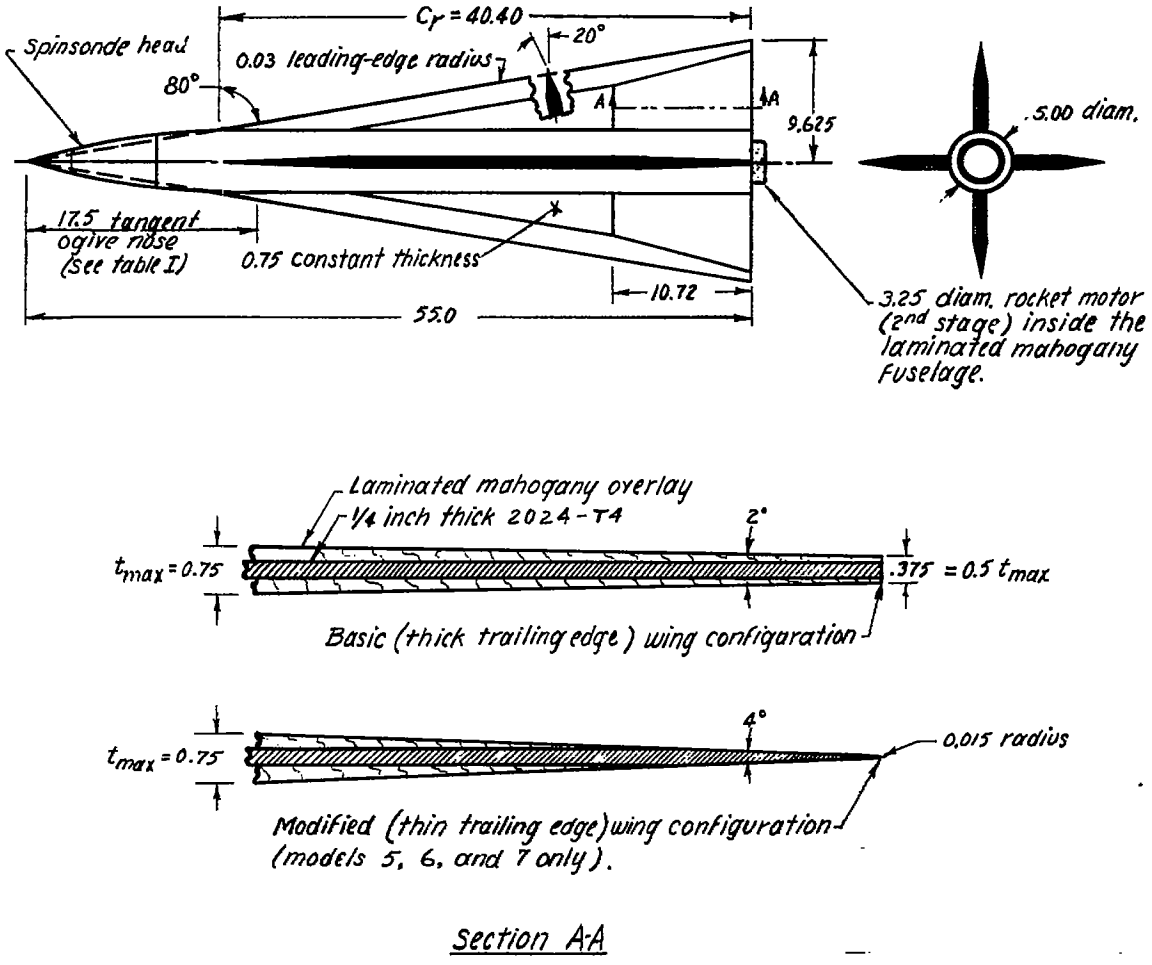

Figure 2.- Geometric and structural details of wings and cylindrical fuselage combination. All dimensions in inches.

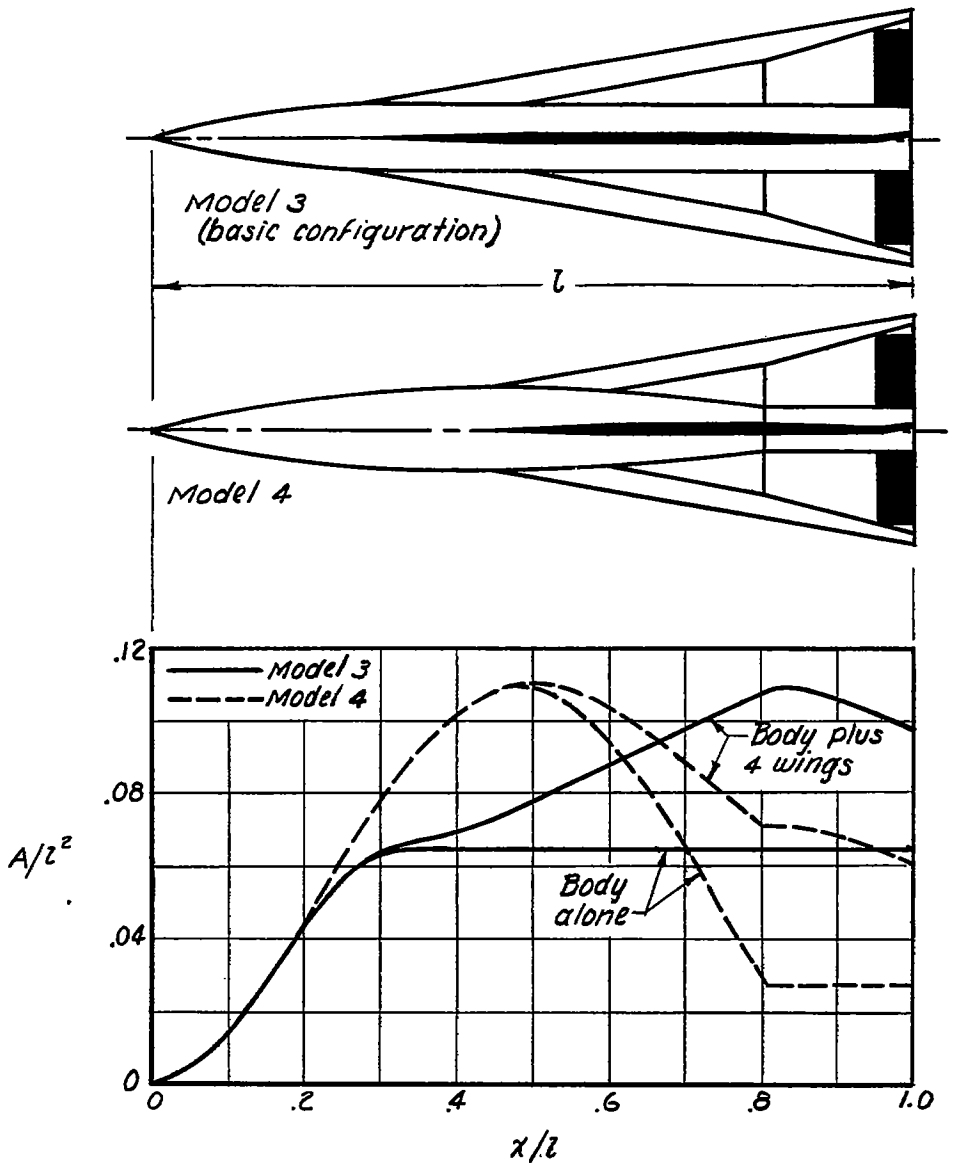

Figure 3.- Variation of model cross-sectional area with model length for basic and modified fuselage configurations. l = 4.58 ft.

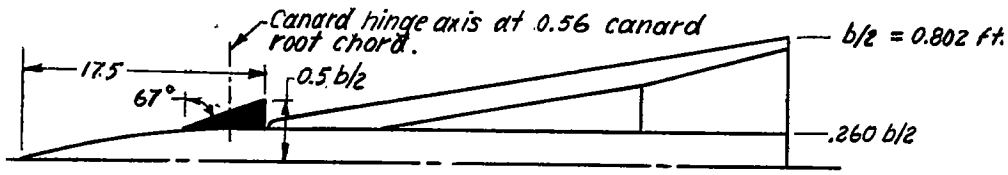

Model 1.- Inline canards ; $\delta_c = 6.06°$.

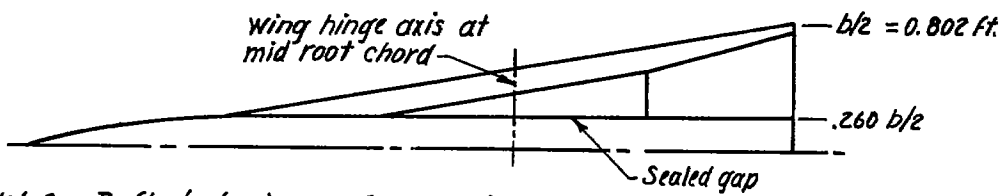

Model 2.- Deflected wings ; $\delta_w = 0.67°$.

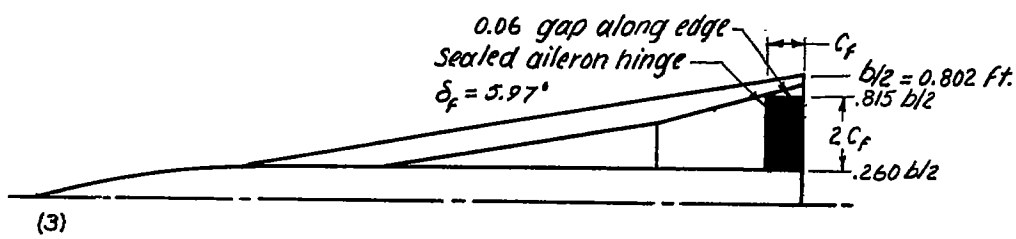

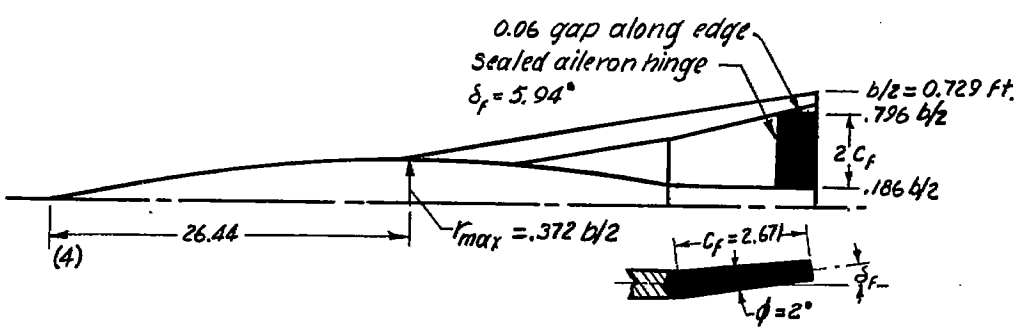

Models 3 and 4.- Plain flaps on basic and modified body shapes; body coordinates listed in table I.

Figure 4.- Geometric details of roll-control configurations. Wings have thick trailing edges $(0.5t_{max})$ unless otherwise noted. Dimensions are in inches.

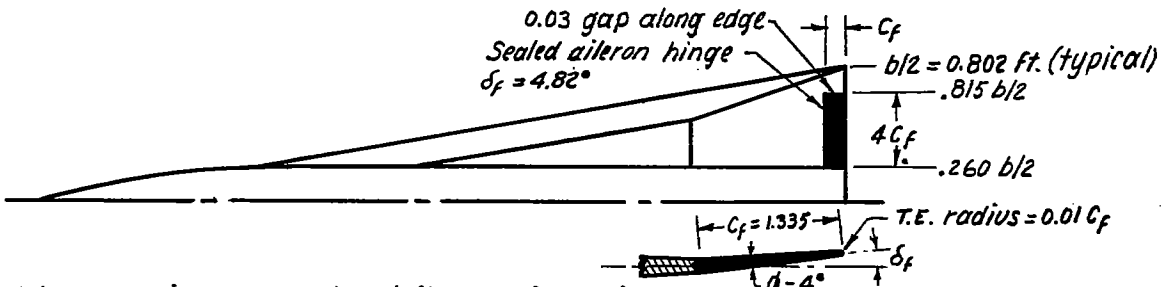

Model 5 .-Plain narrow-chord flap; thin trailing edge.

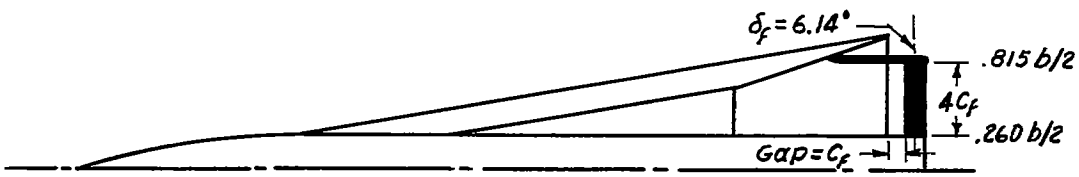

(6)

(7)

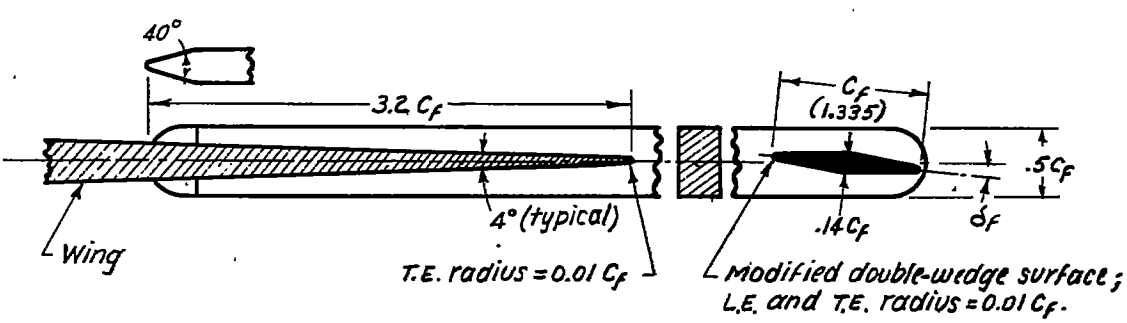

Typical section A-A

Models 6 and 7.- Detached surfaces behind wing trailing edge.

Figure 4.- Continued.

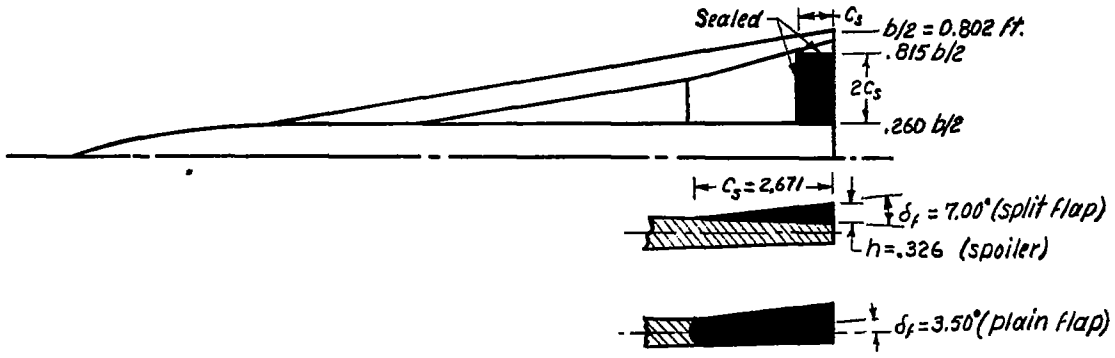

Model 8.- Split flap, ramp spoiler, or thick T.E. plain flap.

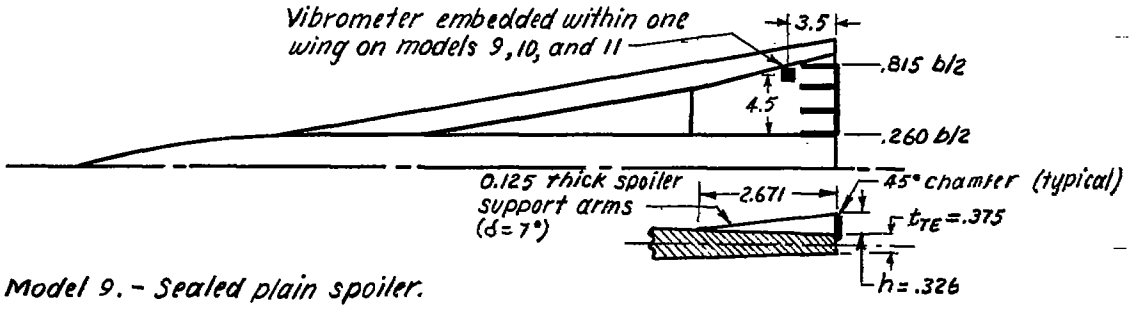

Model 9.- Sealed plain spoiler.

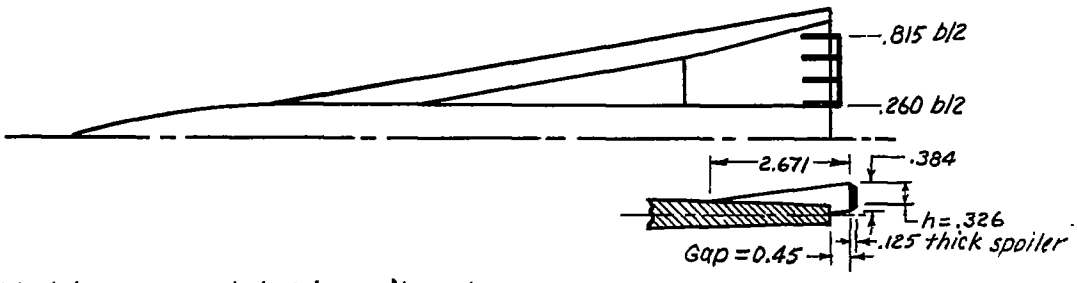

Model 10.- Unsealed plain spoiler at 1.01 C_r.

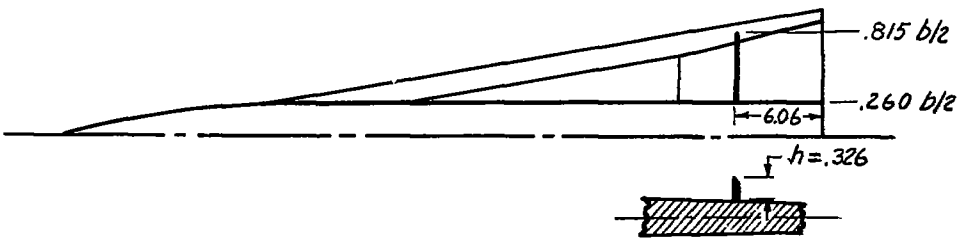

Model 11.- Plain spoiler at 0.85 C_r.

Figure 4.- Continued.

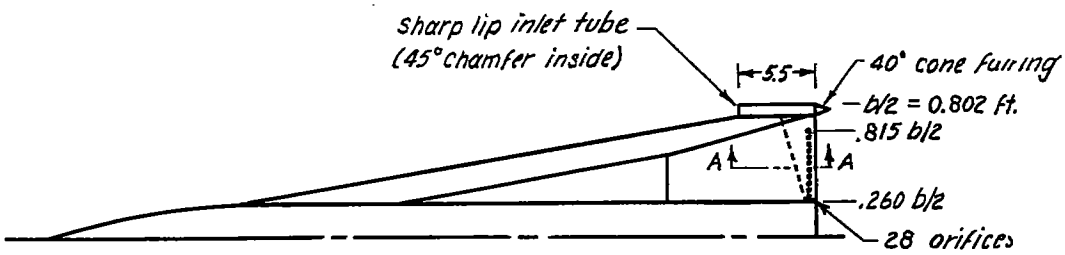

Model 12.- (A_j/A_i = 0.72).

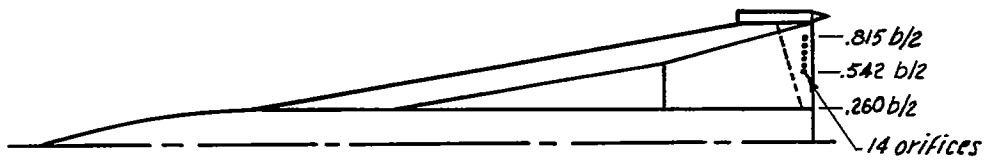

Model 13.- (A_j/A_i = 0.36).

Model 14.- (A_j/A_i = 0.36).

Control details

Orifice diam.	0.129
Orifice spacing	0.1875
No. of orifices	28, 14
Inlet inside diam.	0.805
Inlet outside diam.	0.875

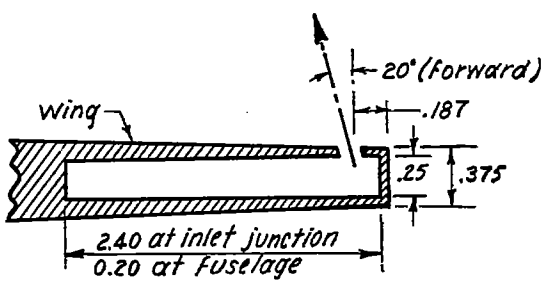

Typical section A-A thru orifice

Inlet-airjet devices.- Jets blowing approximately normal to wing surface; A_i = 0.0019S (total).

Figure 4.- Continued.

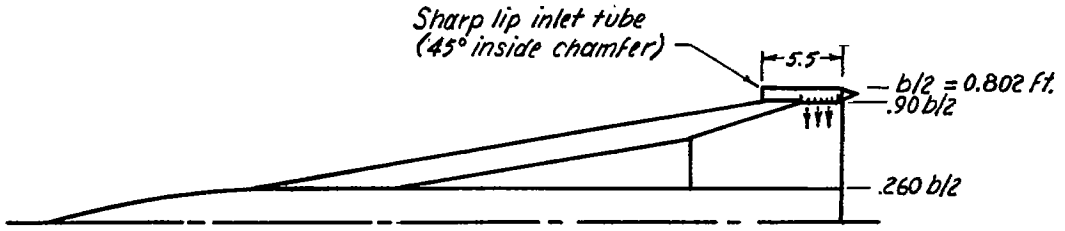

Control variables

Model	h_1	h_2	$\frac{A_j}{A_i}$
15	0.22	0	1.0
16	.11	0	.5
17	.14	.08	1.0

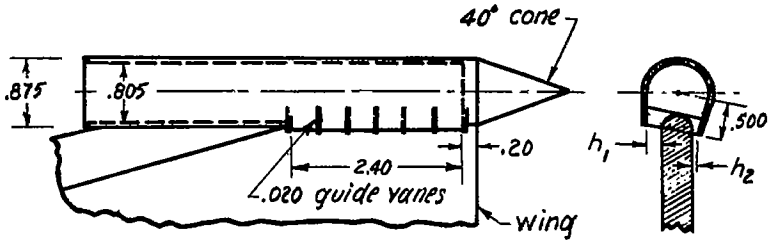

Models 15, 16 and 17.- Inlet-jet; jet blowing spanwise inward; $A_i = 0.0019S$ (total).

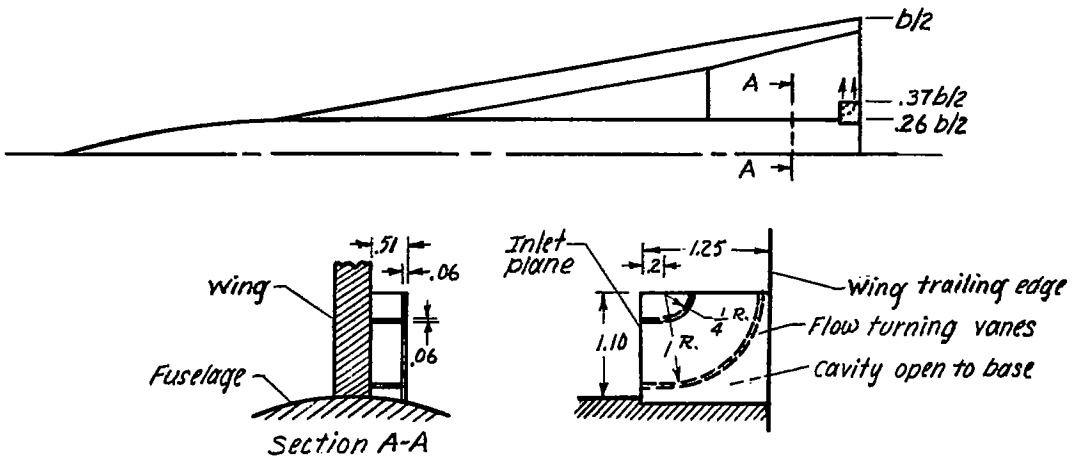

Model 18.- Jet blowing spanwise outward; $A_i = 0.0019S$ (total).

Figure 4.- Concluded.

CONFIDENTIAL

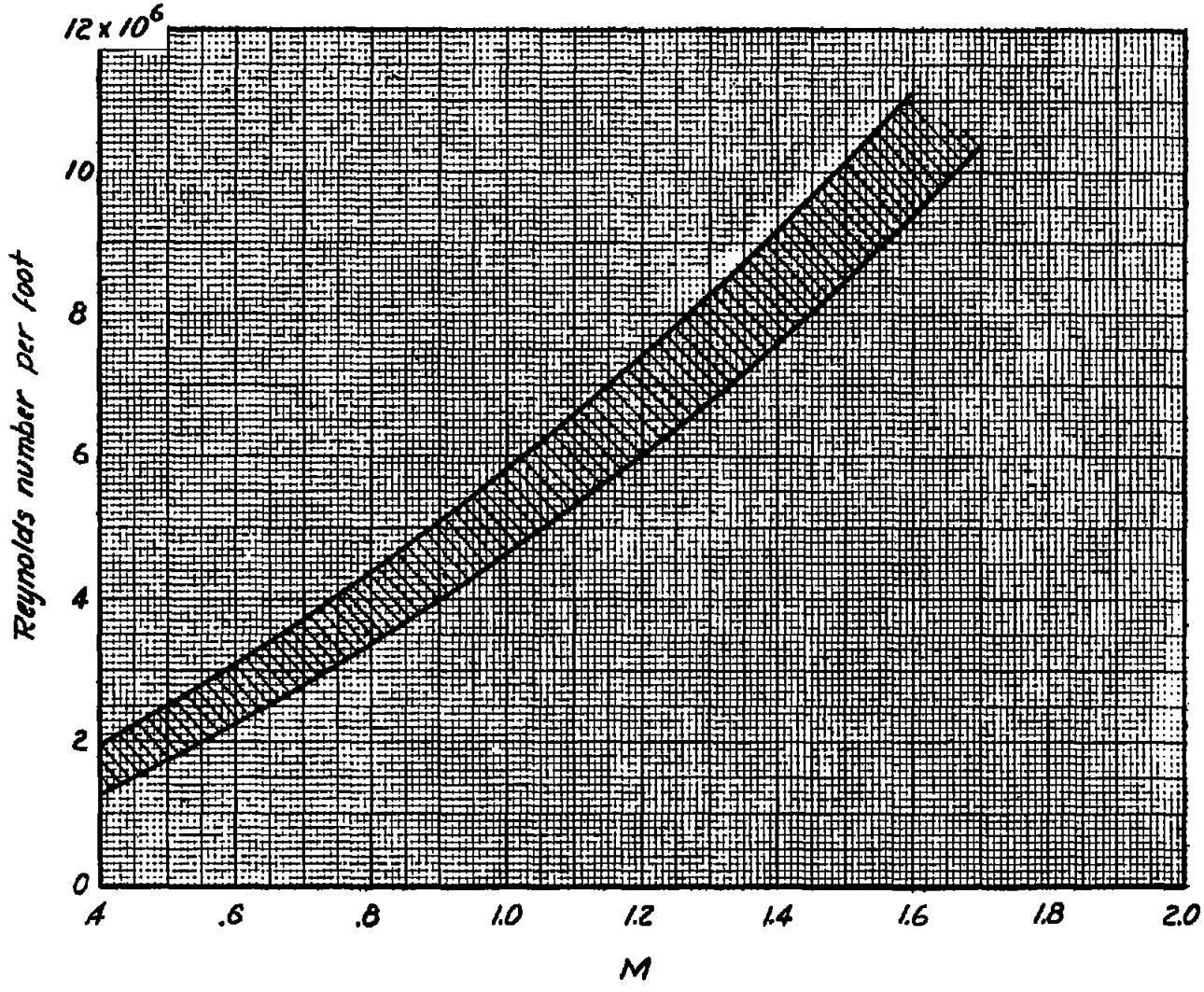

Figure 5.- Range of Reynolds number variation with test Mach number for all test configurations.

CONFIDENTIAL

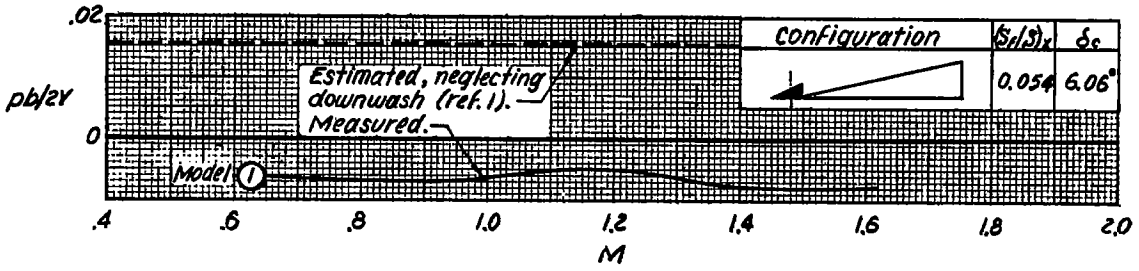

Figure 6.- Variation with Mach number of the rolling effectiveness of differentially deflected inline canard surfaces; $\Lambda_c = 67^\circ$; $(y_o)_c = 0.5b/2$.

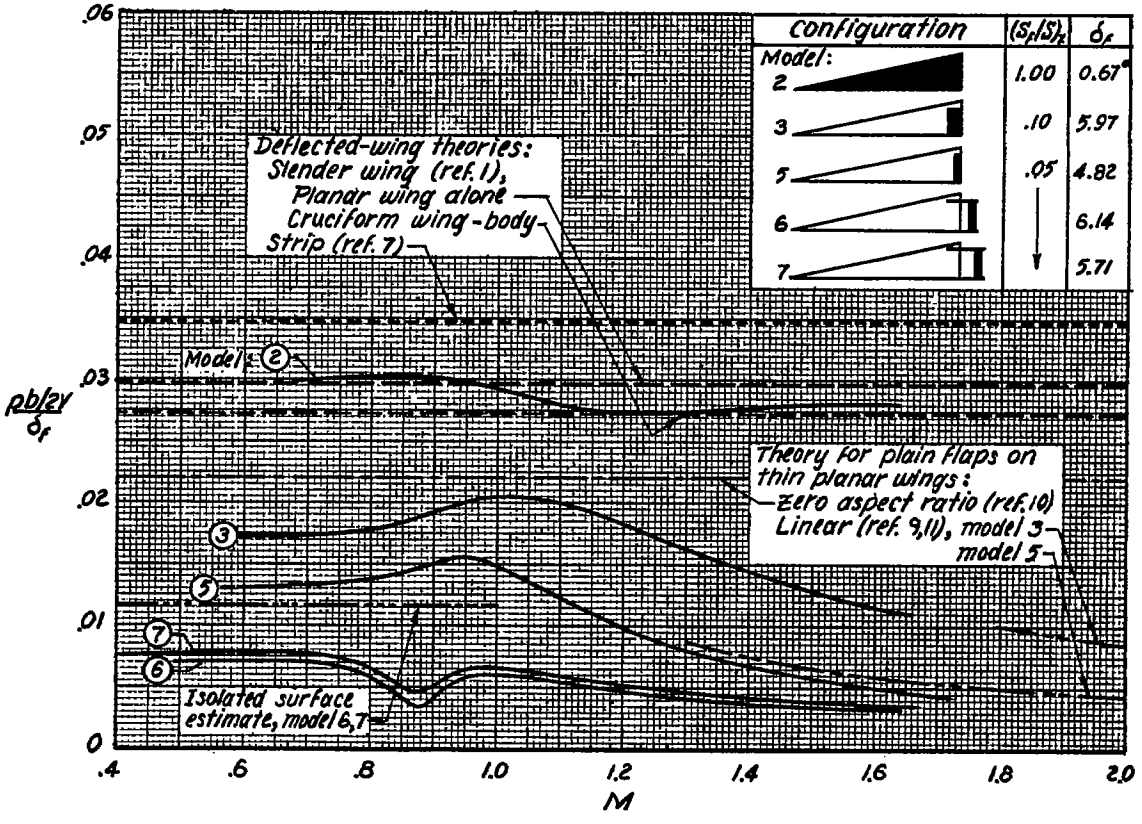

Figure 7.- Variations with Mach number of the rolling effectiveness per degree deflection for deflected wings and flap surfaces. Models 2 and 3 have thick-trailing-edge wings, 5, 6, and 7 thin-trailing-edge wings. $(y_i)_f = 0.26b/2$; $(y_o)_f = 0.82b/2$.

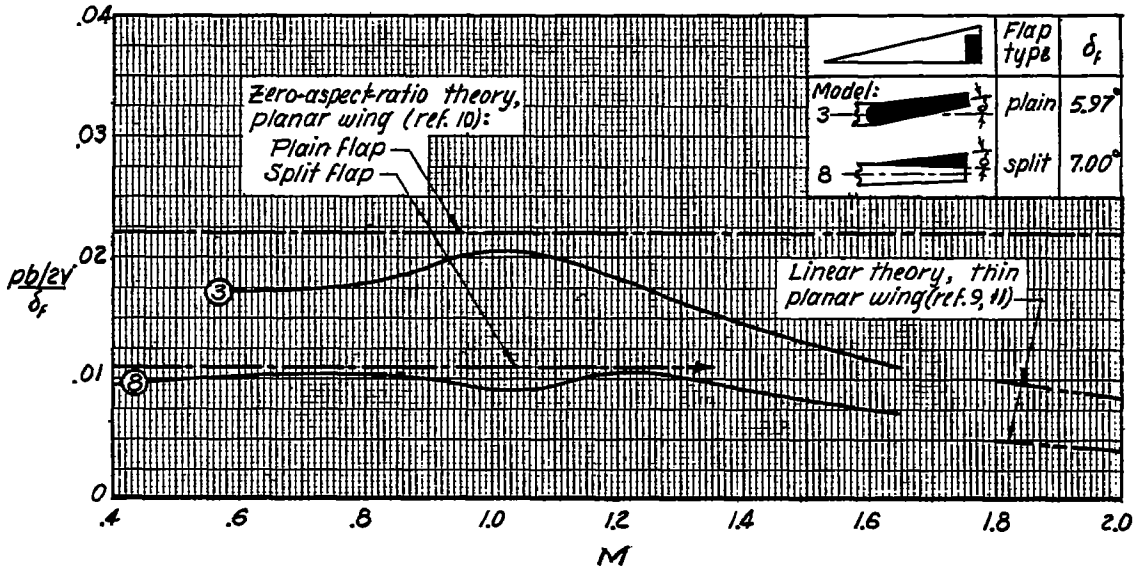

Figure 8.- Comparison of the rolling effectiveness of plain and split flaps. Constant flap chord and flap span; $y_i/\frac{b}{2} = 0.26$; $y_o/\frac{b}{2} = 0.82$; $(S_f/S)_x = 0.10$.

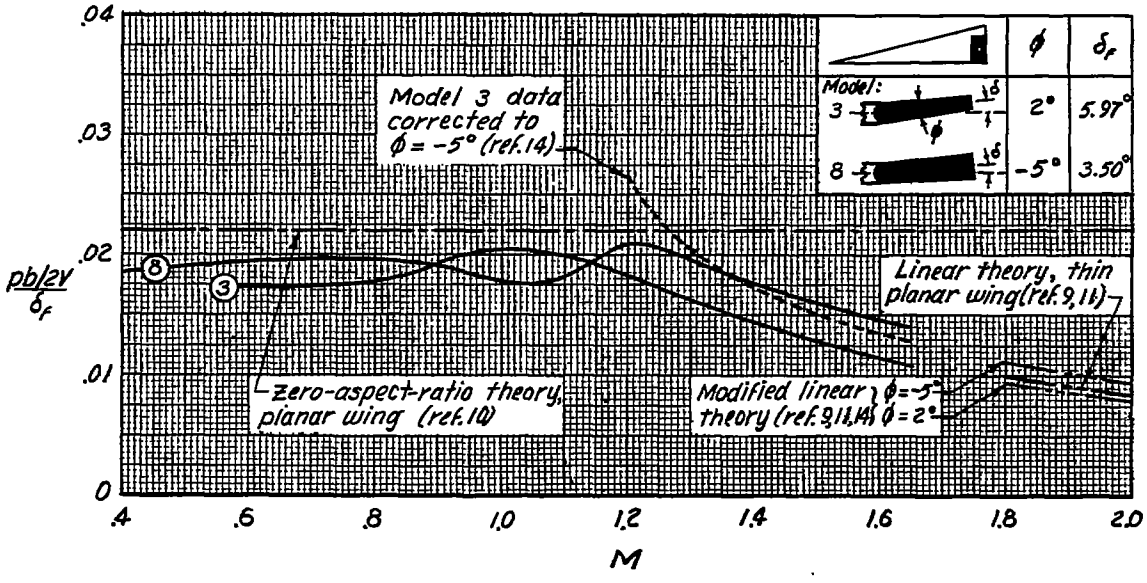

Figure 9.- Effect of increased flap-trailing-edge thickness on rolling effectiveness. $y_i/\frac{b}{2} = 0.26$; $y_o/\frac{b}{2} = 0.82$; $(S_f/S)_x = 0.10$.

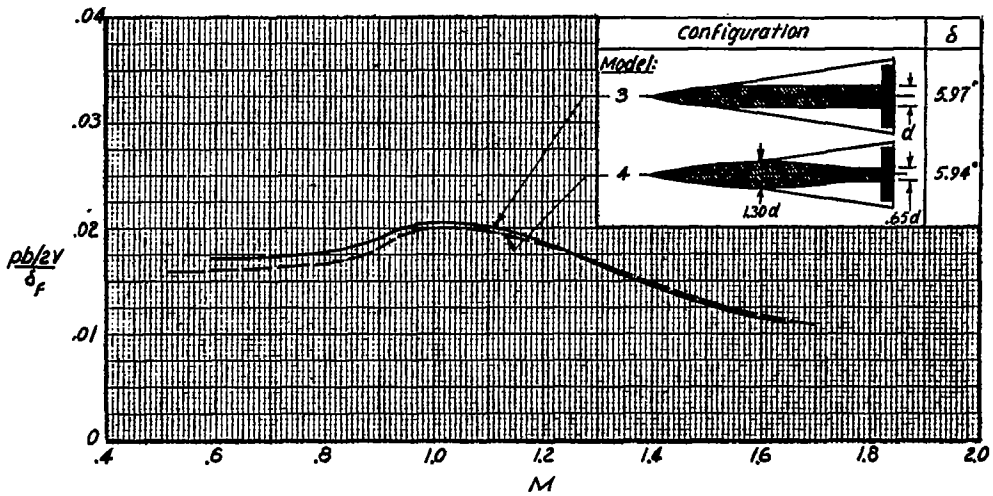

Figure 10.- Effect of a body shape modification on plain flap rolling effectiveness. Constant flap chord, flap span, and exposed wing span; d = 5.00 in.

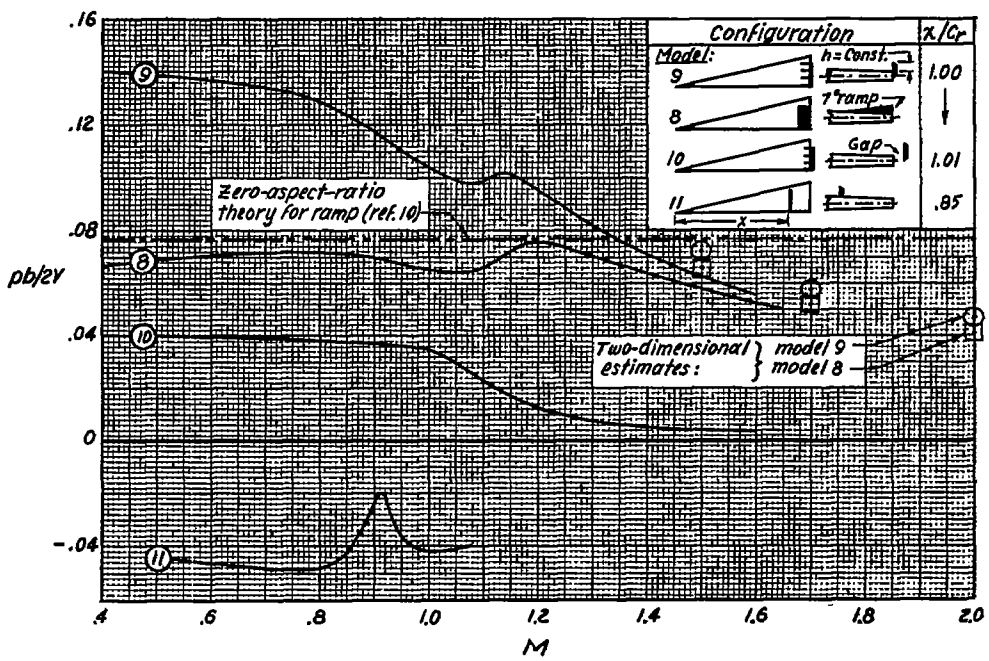

Figure 11.- Variation of rolling effectiveness with Mach number for spoiler controls showing effect of type and chordwise location. $y_i/\frac{b}{2} = 0.26$; $y_o/\frac{b}{2} = 0.82$; $h = 0.008c_r = 0.87t_{TE}$.

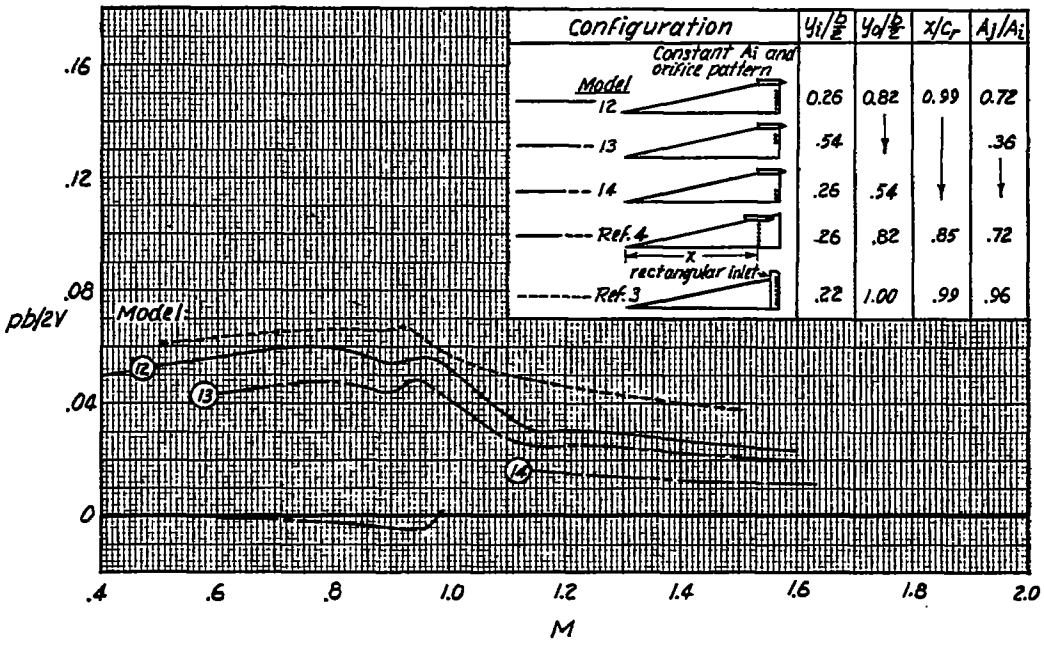

Figure 12.- Variations with Mach number of the rolling effectiveness of air jets blowing approximately normal to the wing surface using air obtained from simple inlets. Orifice diameter, $d_j = 0.0134b/2$; orifice spacing, $\Delta l = 1.46d_j$ on centers; inlet area, $A_i = 0.0019S$.

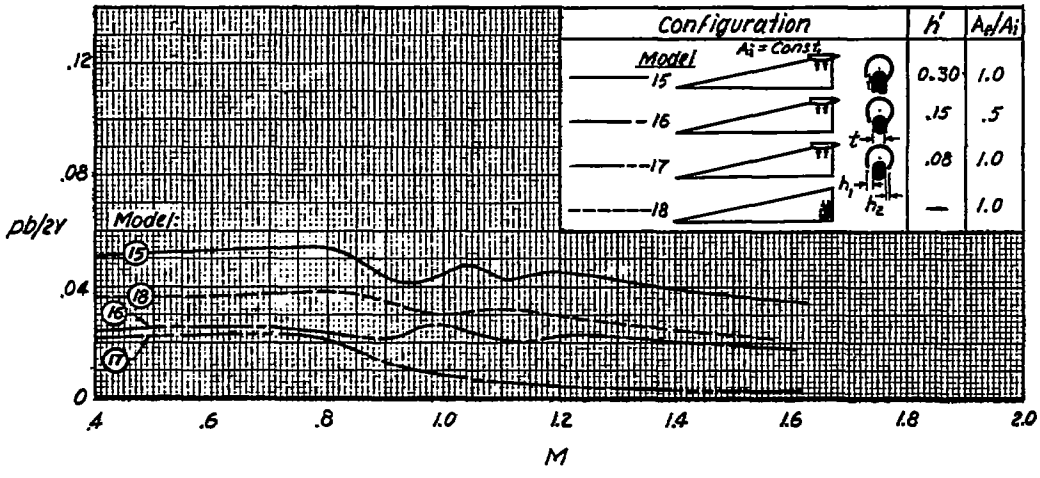

Figure 13.- Variations with Mach number of the rolling effectiveness of air jets blowing spanwise over the wing surface using air obtained from simple inlets. Inlet area, $A_i = 0.0019S$; net exit-port width, $h' = (h_1 - h_2)/t_{max}$.

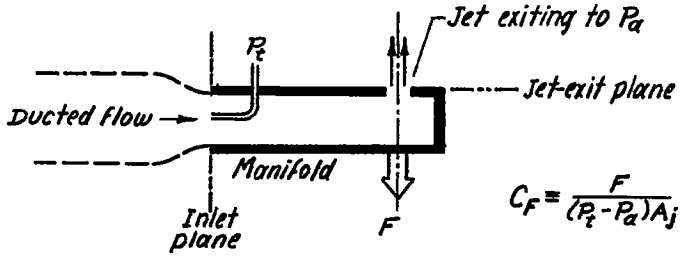

(a) Schematic sketch showing inlet-jet test setup for determining C_F.

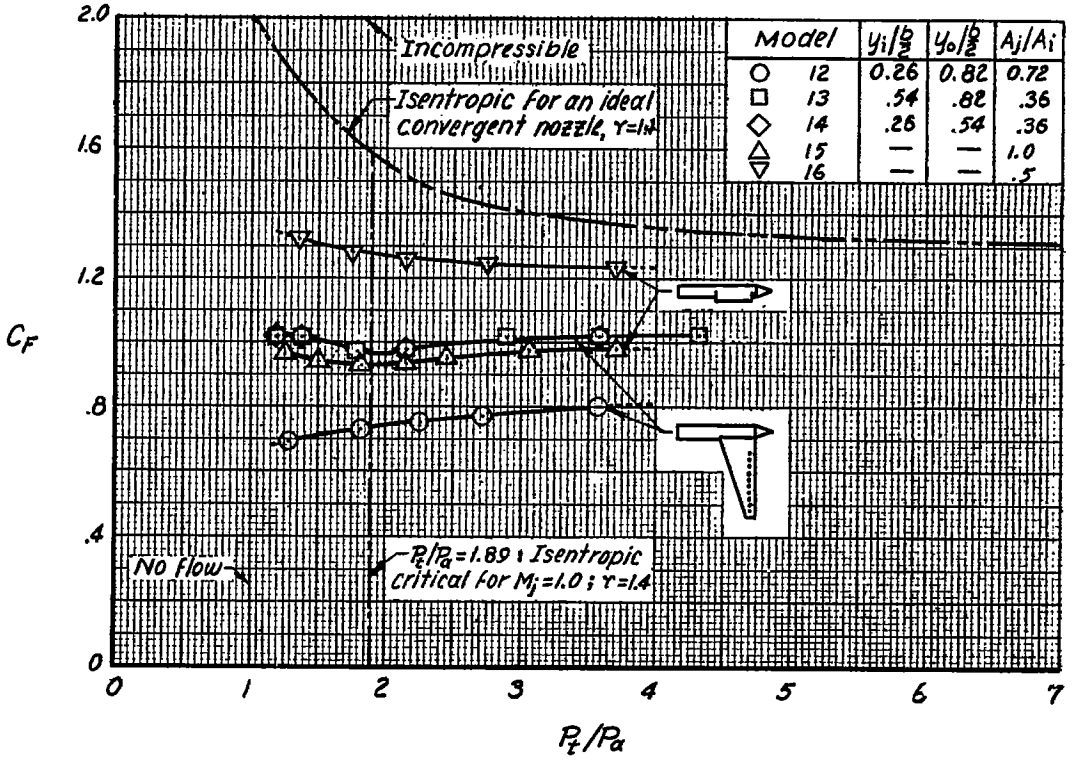

(b) Effect of inlet stagnation pressure ratio on C_F for present-test jet configurations.

Figure 14.- Jet thrust coefficients derived from force tests of various inlet-jet orifice arrangements. A_i = 0.508 sq in.

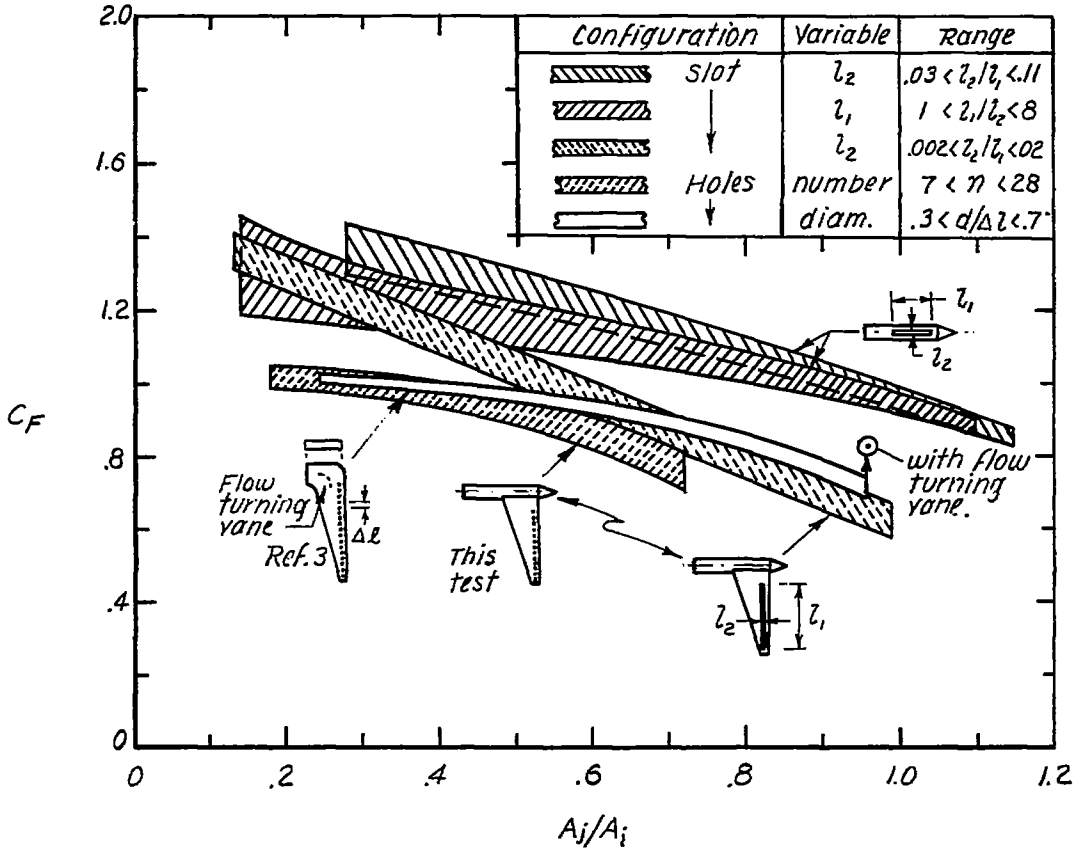

(c) Effect of ratio of exit area to inlet area on C_F for the range:

$$1.2 < \frac{P_t}{P_a} < 4.0.$$

Figure 14.- Concluded.

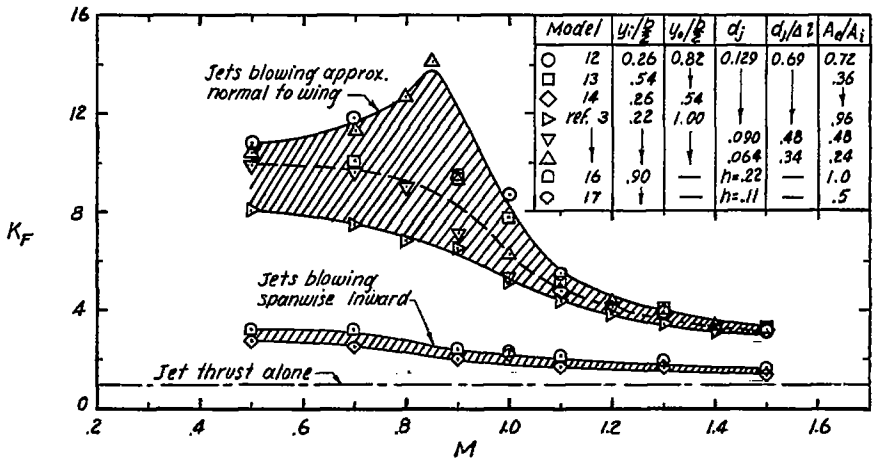

(a) Values of K_F for present and reference 3 test configurations employing inlet-jet roll-control devices near the trailing edge of 80° delta wings at zero lift. Inlet areas, A_i and jet orifice spacing, Δl are constants.

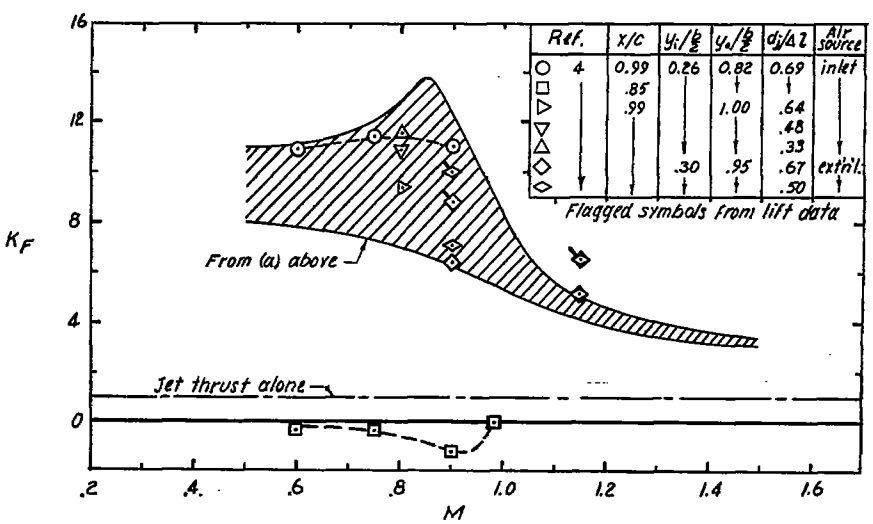

(b) Comparison, for vertically blowing jets on 80° delta wings, of K_F from figure 15(a) with values derived from referenced rolling moment and incremental-lift data near zero lift.

Figure 15.- Variations with Mach number of the thrust-force magnification obtained with several wing-jet combinations. Jet thrust is assumed to act normal to wing chord plane.

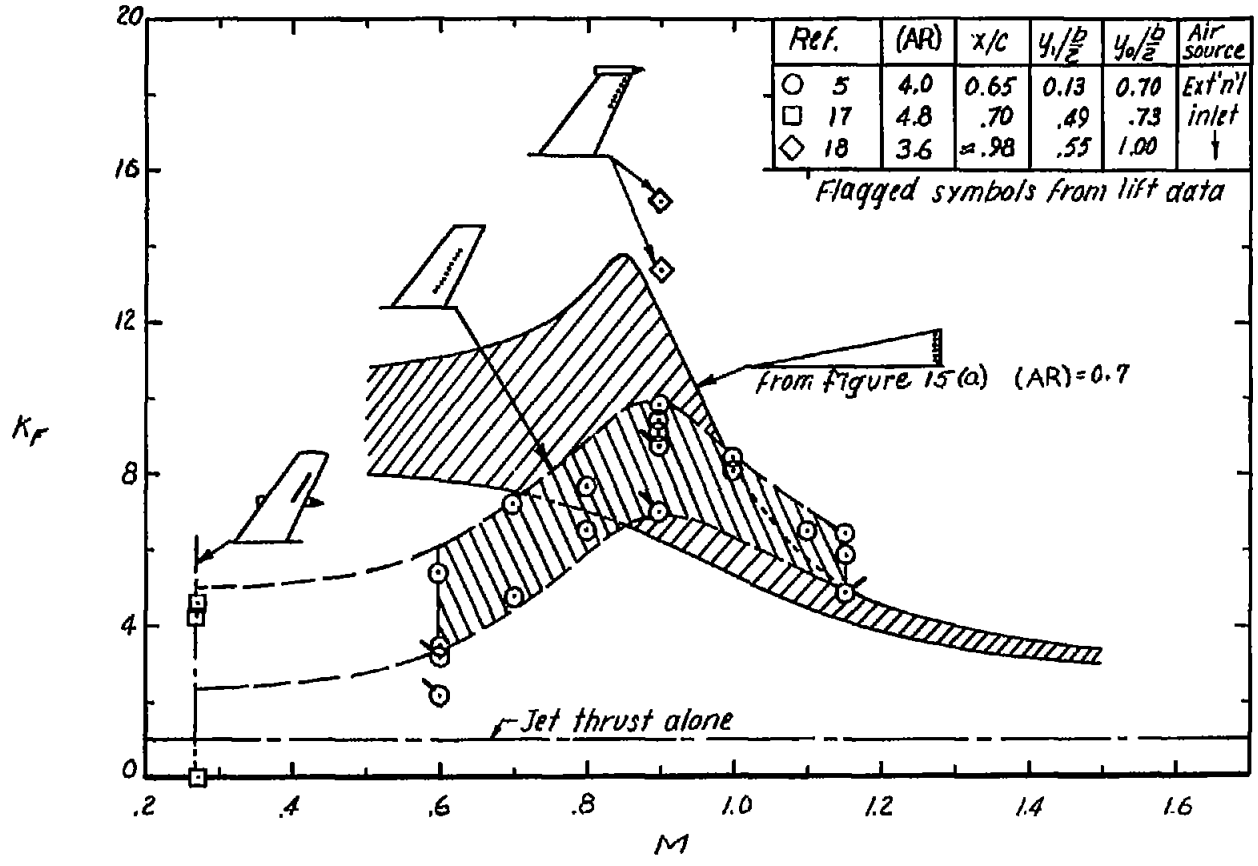

(c) Some effects on K_F of jet chordwise location for other wings and a comparison of results with values derived from data on 80° delta wings. Values of K_F for referenced configurations were determined from both rolling moment and incremental-lift information taken near zero lift ($\alpha \lessapprox \pm 4^{\circ}$).

Figure 15.- Concluded.

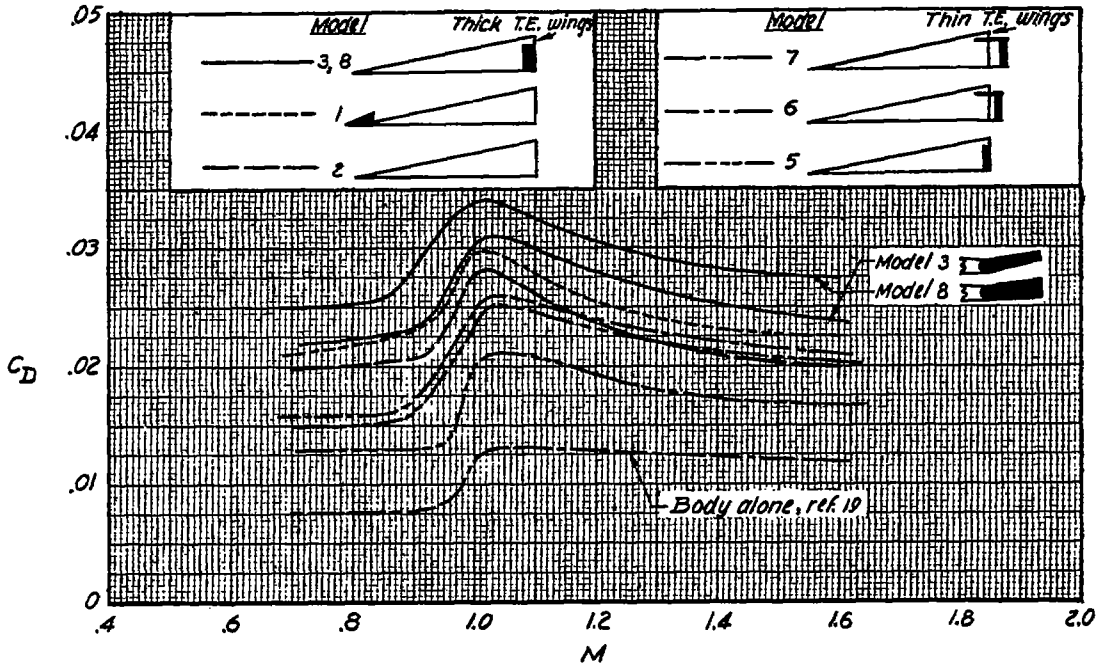

Figure 16.- Variations with Mach number of the total drag coefficient o. body-alone and present-test configurations with deflected-surface-type controls.

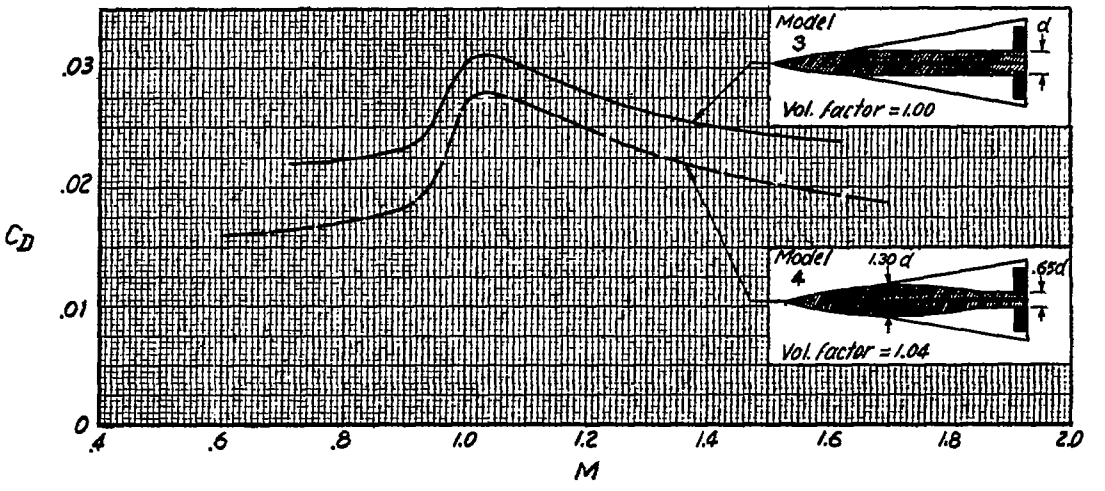

Figure 17.- Effect of a fuselage modification on the total drag of a plain-flap-controlled configuration. Equal maximum cross-sectional areas; fuselage volume factor relative to volume of model 3 fuselage; $\delta_f \approx 6.0^\circ$.

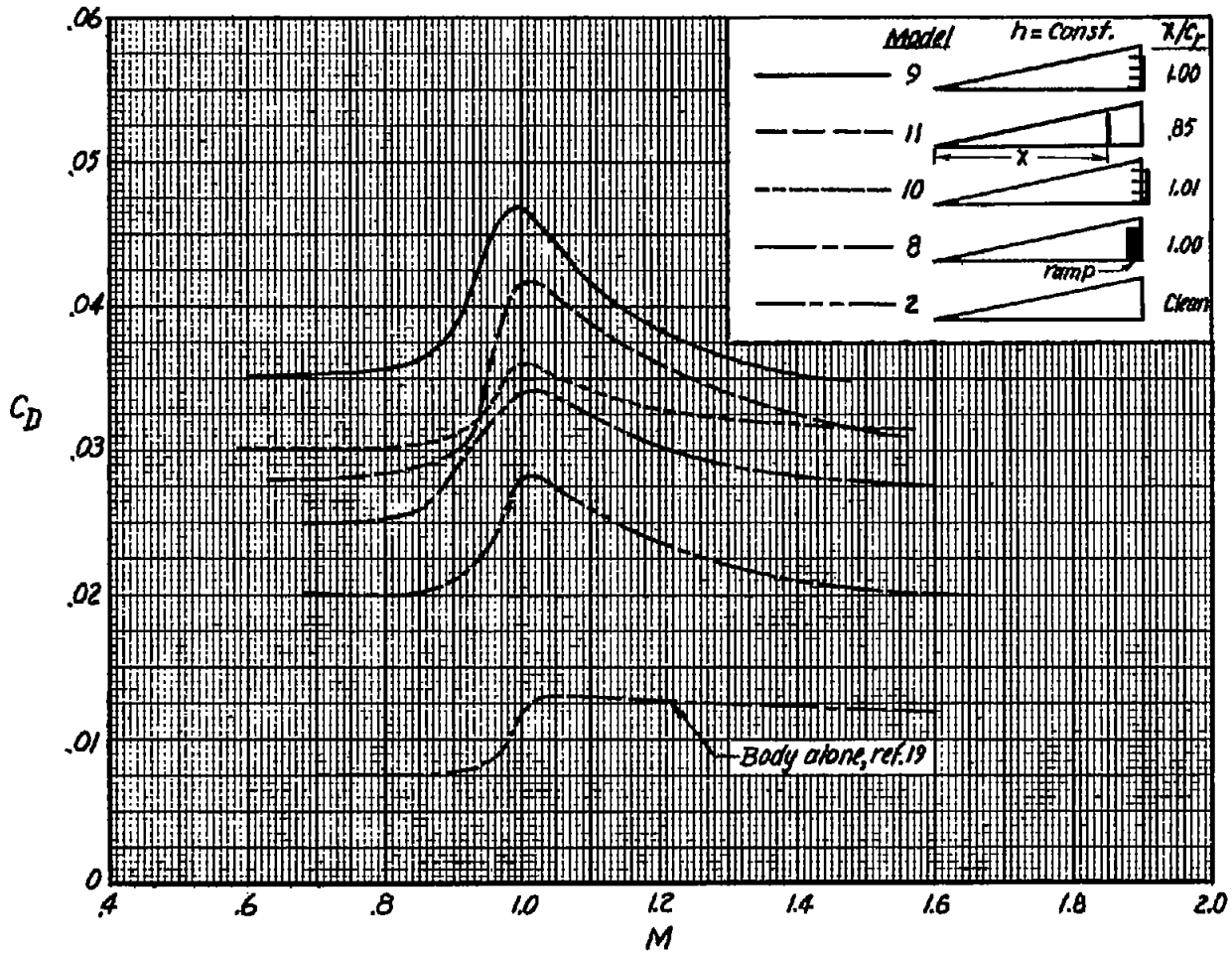

Figure 18.- Variations with Mach number of the total drag coefficients of the spoiler-controlled configurations. $y_i/\frac{b}{2} = 0.26$; $y_o/\frac{b}{2} = 0.82$; $h_s = 0.008c_r = 0.87t_{TE}$.

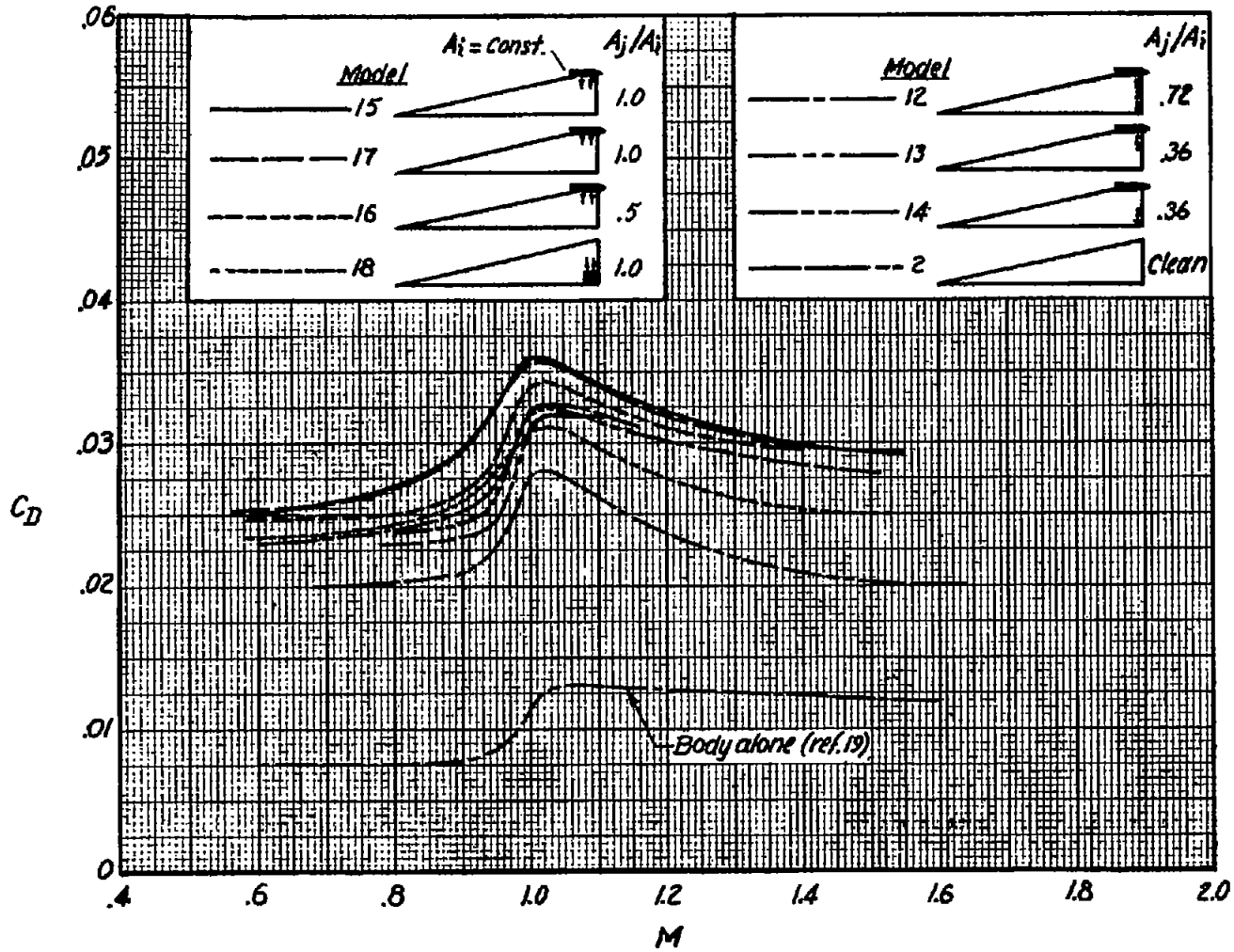

Figure 19.- Variations of total drag coefficient with Mach number for the jet-controlled test configurations.

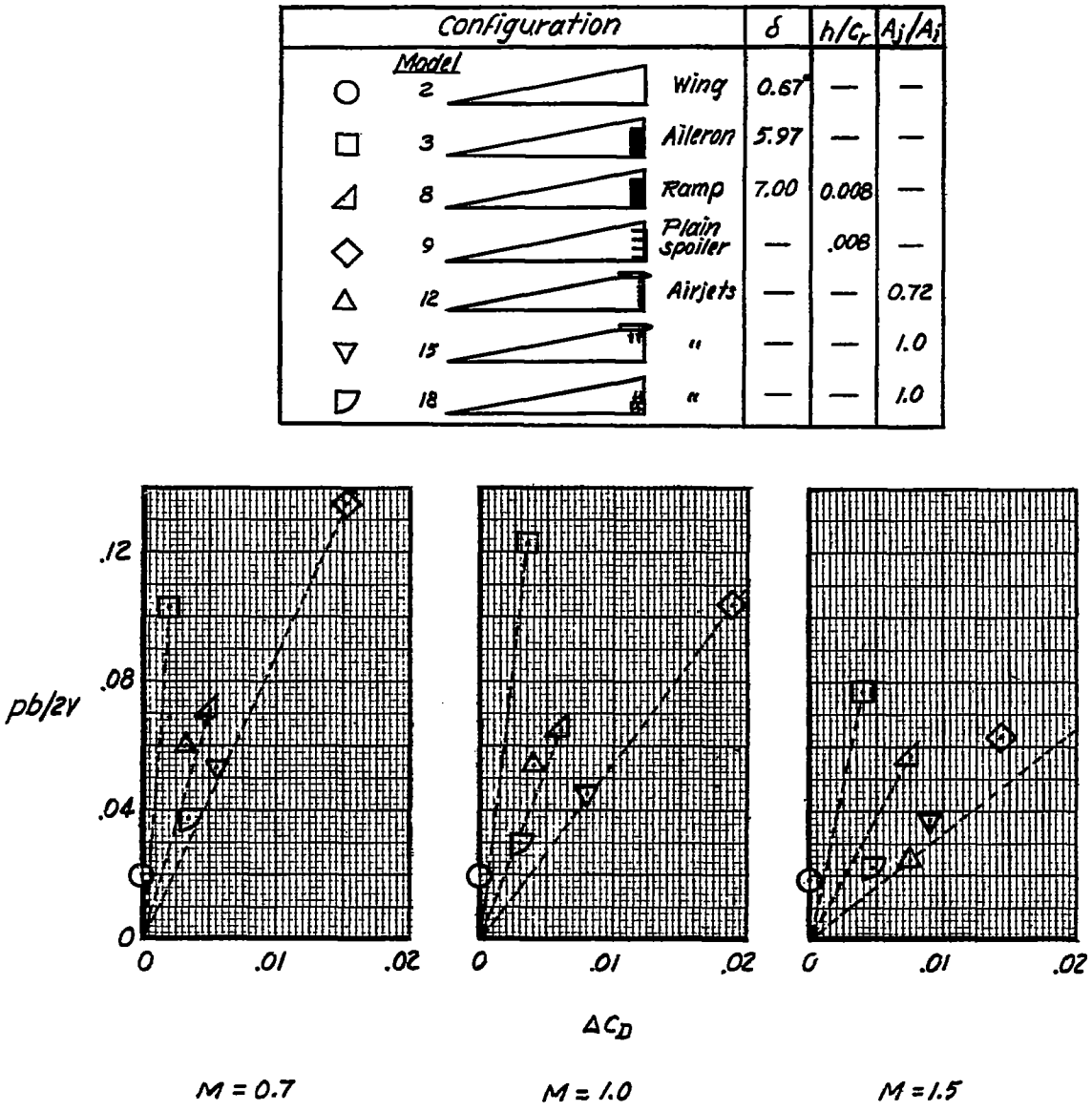

Figure 20.- Correlation of measured rolling effectiveness with incremental drag coefficient, ΔC_D for various controls. ΔC_D based on total exposed wing area; thick-trailing-edge wing configurations.